Optimal cues for transmission investment in malaria parasites

Avril L. Wang[1¤*], Megan A. Greischar[2], Nicole Mideo[1]

1 Department of Ecology and Evolutionary Biology, University of Toronto, Toronto, Ontario, Canada
2 Department of Ecology and Evolutionary Biology, Cornell University, Ithaca, New York, United States

¤Current Address: Department of Biology, Massachusetts Institute of Technology, Cambridge, Massachusetts, United States
* avril137@mit.edu

Abstract

The timing of investment into reproduction is a key determinant of lifetime reproductive success (fitness). Many organisms exhibit plastic, i.e., environmentally-responsive, investment strategies, raising the questions of what environmental cues trigger responses and why organisms have evolved to respond to those particular cues. For malaria parasites (*Plasmodium spp.*), investment into the production of specialized transmission stages (versus stages that replicate asexually within the host) is synonymous with reproductive investment and also plastic, responding to host- and parasite-derived factors. Previous theory has identified optimal plastic transmission investment strategies for the rodent malaria parasite, *P. chabaudi*, as a function of the time since infection, implicitly assuming that parasites have perfect information about all aspects of the within-host environment and how it's changing. We extended that theory to ask which cue(s) enable plastic transmission investment strategies that maximize parasite fitness, quantified as host infectiousness during acute infection. Our results show that sensing parasite-associated cues—the abundance of infected red blood cells or transmission stages—allows parasites to achieve fitness approaching that of the optimal time-varying strategy, but only when parasites perceive the cue non-linearly, responding more sensitively to changes at low densities. This scaling allows parasites to delay transmission investment at the onset of infection, a crucial feature of the optimal strategy, since parasite abundance rises orders of magnitude over the first days of infection. However, no single cue can recreate the best time-varying strategy or allow parasites to adopt terminal investment as the infection ends, a classic expectation for reproductive investment. Sensing two cues —log-transformed infected and uninfected red blood cell abundance —enables parasites to accurately track the progression of the infection, permits terminal investment, and recovers the fitness of the optimal time-varying investment strategy. Importantly, parasites that detect two cues more efficiently exploit hosts, resulting in higher virulence compared with those sensing only one cue. Finally, our results suggest a potential tradeoff between achieving an optimal transmission investment strategy at a given age of infection and robustness in the face of environmental or developmental fluctuations.

Introduction

A key goal of life history theory is understanding how organisms should invest in reproduction over the course of their lives and explaining the substantial variation in patterns observed (e.g., [1]). Reproductive investment entails a resource allocation tradeoff: resources allocated to growth cannot, generally, also be allocated to reproduction. Classic work predicts that the resolution to this tradeoff will change with the age of an organism, increasing as the time left for reproduction declines [2, 3], or its "state," a combination of intrinsic, physiological factors and external, environmental ones [4]. Experimental data have shown that investment can be plastic, where organisms' age and state can independently shape reproductive efforts to maximize lifetime fitness (e.g., [5, 6]). How organisms estimate the time remaining for reproduction—that is, what cues they utilize from their own physiology and the environment—remains an open question.

For sexually-reproducing parasites, patterns of reproductive investment can have clinical and epidemiological consequences. Protozoan parasites of *Plasmodium* spp. —the etiological agents of malaria —infect the red blood cells of their host, and a given infected cell will either produce more asexual, cell-infecting stages ("growth" of an infection) or produce a single gametocyte, a sexually-differentiated stage that can be transmitted to mosquito vectors (potentially "reproducing" an infection). The proportion of infected cells that produce transmissible gametocytes (known in the malaria literature as the "conversion rate") is a measure of investment in reproduction/transmission. This trait has a direct link to infectiousness, since more gametocytes means greater chance of onward transmission to a biting mosquito [7–9] and can influence the virulence or severity of infection, since all else equal, lower transmission investment means more host-damaging asexual parasites are produced [10].

In line with standard predictions from life history theory, for malaria parasites it is postulated that mild stressors should promote reproductive restraint, while strong stressors that signal imminent clearance should lead to complete investment in transmission [10], i.e., terminal investment [11]. But "stress" will vary over the course of infection, as parasites deplete host resources and hosts respond via immunity. These dynamics could explain why transmission investment in malaria parasites is variable over the lifespan of infections (i.e., plastic) [12–16]. Mathematical models assessing the fitness consequences of different patterns of transmission investment demonstrate that the best strategy involves initial reproductive restraint that facilitates within-host parasite population growth (rather than early investment in gametocytes that have very low likelihood of onwards transmission due to low parasite densities), followed by an increase in investment once parasite densities have risen, culminating in terminal investment as the infection is ending [15]. This work assumes that transmission investment is a function of the age of infections, about which parasites have perfect knowledge. The implicit assumptions are that all infections proceed identically, a problem common to models of age-specific reproductive investment [17], and that infection age is a perfect proxy for state. These assumptions limit the ability to predict the influence of novel perturbations, like vaccination, on transmission investment and infection outcomes.

In this study, we extend a previously-published model of within-host malaria infection dynamics to include transmission investment as a function of environmental cues, i.e., components of state. We focus on the dynamics of the model rodent malaria parasite *Plasmodium chabaudi* given the availability of tools to quantify transmission investment [15] and manipulate host "state," which enables future experimental testing

of parasite cue perception. In our model, different cues may give rise to different early patterns of transmission investment, thus altering the trajectory of infections, which feedback to influence the subsequent expression of the trait. We use numerical optimization to determine the best response for each cue (i.e., the optimal reaction norm) and compare the maximum fitness achieved across cues over the course of an infection. We show that the choice of cue affects both the dynamics of transmission investment and parasite fitness. Sensing logged parasite density enables parasites to delay transmission investment, but it is insufficient for achieving terminal investment; instead, dual cue perception is necessary. Interestingly, we note a potential tradeoff between state differentiation and cue robustness, highlighting the constraints imposed on attaining optimal strategies in natural systems. Lastly, we demonstrate that environmental cue perception is an important mediator of parasite virulence and discuss its implications for parasite evolution. In summary, our study further characterizes plasticity in *P. chabaudi* life history, while introducing a mathematical framework that explicitly incorporates cue perception that could be broadly applied to other organisms.

Results

We use mathematical modeling to investigate which within-host environmental cues malaria parasites "should" sense for determining transmission investment (i.e., which cues give rise to the highest parasite fitness) and the optimal shape of the relationship between each cue and transmission investment (i.e., the optimal reaction norms). Our mathematical model tracks within-host dynamics of infection with the rodent malaria parasite *P. chabaudi* (Fig 1A). Asexual parasites, called merozoites (M), invade uninfected red blood cells (RBCs; R), which can go on to produce more merozoites that are either asexually-committed (M; if these merozoites infect an RBC, they will produce more merozoites) or sexually-committed (M_g; if these merozoites infect an RBC, they will produce a gametocyte, G). RBCs infected with these different types of merozoites are denoted as I and I_g, respectively. Importantly, the proportion of all infected cells that follow these different developmental routes (producing M or M_g) defines transmission investment. While previous approaches have treated this trait as either fixed or time-dependent (e.g., [18–23]), here we explicitly model it as a function of within-host environmental cues (see Materials and Methods). We select as plausible cues various measures of the density of parasites and host resources that have been shown experimentally to impact transmission investment in *Plasmodium* spp. (Table 1). We test both raw densities and logged densities as cues to expand the range of reaction norm shapes explored and because changes in infection dynamics are observed in this system when doses change by orders of magnitude [24].

In our model, cue perception occurs at the beginning of asexual iRBC development (Fig 1B), determining the proportion of asexual iRBCs that produces sexually-committed merozoites. Note that this modeling choice introduces a time lag between sexual commitment (as a result of cue perception) and gametocyte production, which is a departure from previous modeling work [20], but reflects empirical data on the canonical timeline of sexual commitment from the best studied system (*Plasmodium falciparum* [26]). For each putative cue, we define its associated reaction norm using flexible splines. We used a combination of local and global numerical optimization algorithms to find the reaction norm that maximizes the cumulative transmission potential to mosquito vectors over the course of a 20-day infection, as in previous work [20, 27]. To validate the best reaction norm obtained for each cue, we compare the fitness achieved by these putative optimal splines with that achieved by 1000 random splines (S1 Fig). We find that our optimal splines outperform all the random ones,

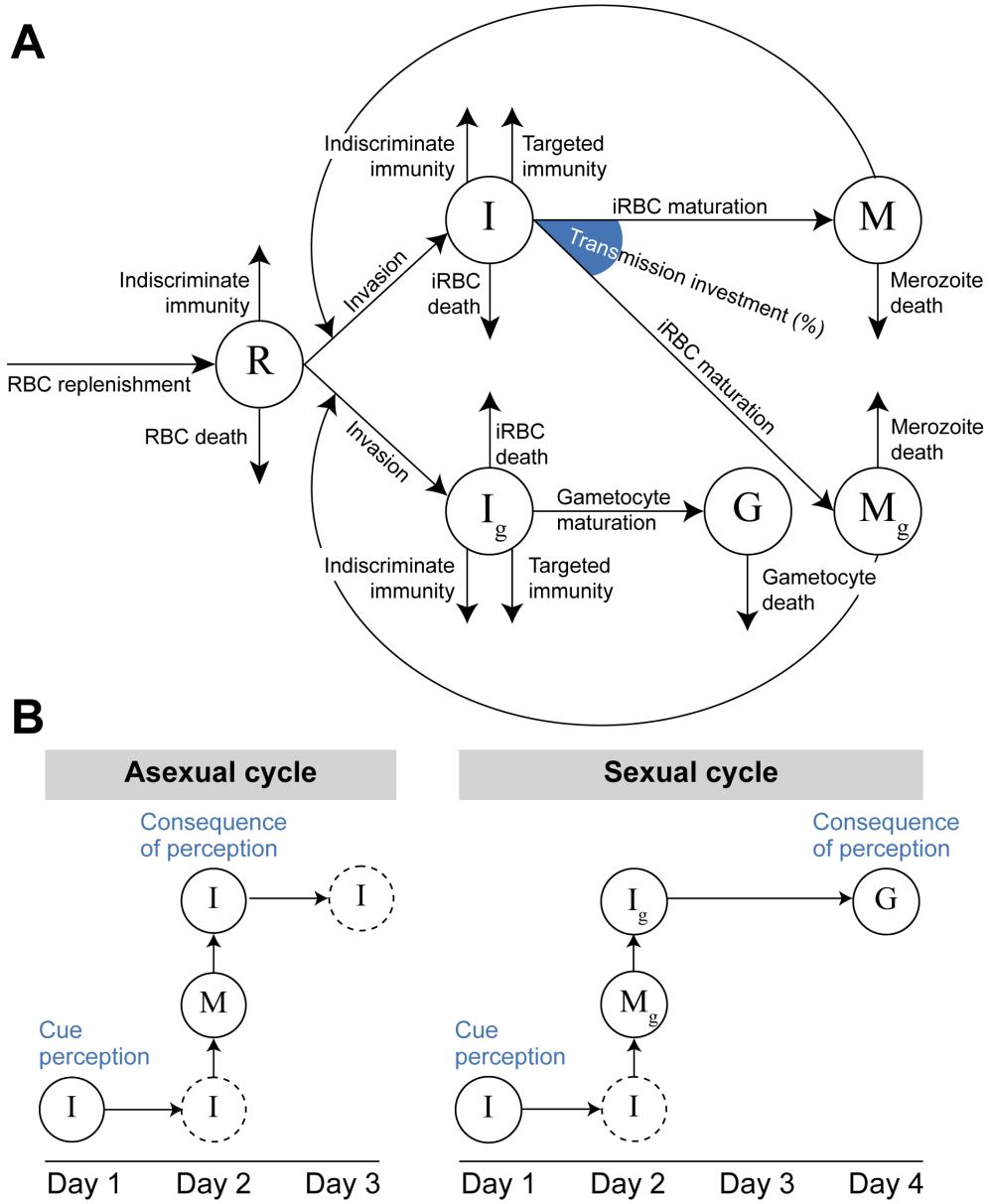

Fig 1. Schematic of *P. chabaudi* within-host infection dynamics. (A) Flow diagram of model tracking the dynamics of red blood cells (R; RBCs), RBCs infected with asexual parasites (I), RBCs infected with sexual—but not yet mature —parasites (I_g), asexually-committed merozoites (M), sexually-committed merozoites (M_g), and gametocytes (G). (B) Temporal dynamics of cue perception. Cue perception occurs one day before the production of asexual/sexual merozoites, thereby introducing a delay between cue perception and the consequences of cue perception (i.e., production of more asexual infected RBCs or gametocytes). A further delay occurs in the sexual cycle since gametocytes of *P. chabaudi* take two days to mature [25]. Dashed circles indicate the bursting/maturation of a particular cohort of iRBCs.

increasing our confidence that the optimizations were successful.

Table 1. Putative within-host environmental cues

Cue	Abbreviation	Experimental Evidence
Infected RBC (iRBC) density		[14, 28, 29]
Asexually-committed	I	
Asexually-committed, $\log_{10}$	I log	
Sexually-committed	Ig	
Sexually-committed, $\log_{10}$	Ig log	
Total (I+Ig)	Total I	
Total (I+Ig) , $\log_{10}$	Total I log	
Gametocyte density		[14, 28, 29]
Gametocytes	G	
Gametocytes, $\log_{10}$	G log	
Resource density		[14, 29]
Uninfected RBC	R	
Uninfected RBC, $\log_{10}$	R log	

Cue perception mediates parasite life history and fitness

Based on previous work modeling *P. chabaudi* transmission investment as a function of time [20], we expect the following as the best strategy over the course of a 20-day infection: parasites should delay investment early on, display a rapid increase in investment when sufficient gametocytes can be produced to ensure transmission, subtly reduce investment in the face of declining resources, and ultimately rise to the highest levels of investment shortly before the end of infection (roughly, "terminal investment" [10, 20]). Although the model we employ here has a few key differences from that work (notably, it includes targeted and indiscriminate immune responses; see Materials and Methods), we find a similar optimal transmission investment pattern as in [20] when we assume that investment is a function of time (Fig 2A). When parasites instead respond to their environment and are constrained to respond to a single within-host cue, these same patterns of transmission investment cannot be fully recapitulated. Consequently, parasite fitness is lower in every case than when the cue is time (Fig 2A).

The environmental cues that result in the highest parasite fitness include logged parasite-centric cues (e.g., $\log_{10}$ densities of sexually-committed iRBCs). The perception of these cues is sufficient to produce the initial delay in transmission investment, but the delay is longer and there is no increase in investment near the end of infection (Fig 2A). Given that parasite densities rise non-linearly at the start of infections (both simulated and real [12, 30–33]), sensing logged rather than raw densities results in reaction norms that are more sensitive to those early changes (Fig 2B), enabling parasites to increase transmission investment after the densities have reached a rough threshold. In contrast, raw parasite density and densities of host resources (RBCs) provide poor cues for those initial stages of infection —in the first case because reaction norms essentially ignore the changes at low early parasite densities (Fig 2B) and in the second case because RBC densities change very little early on —and, therefore, do not allow parasites to engage in delayed transmission investment (Fig 2A). Overall, our results broadly suggest that early transmission delay necessitates an "ultrasensitive" response to changes at low parasite density.

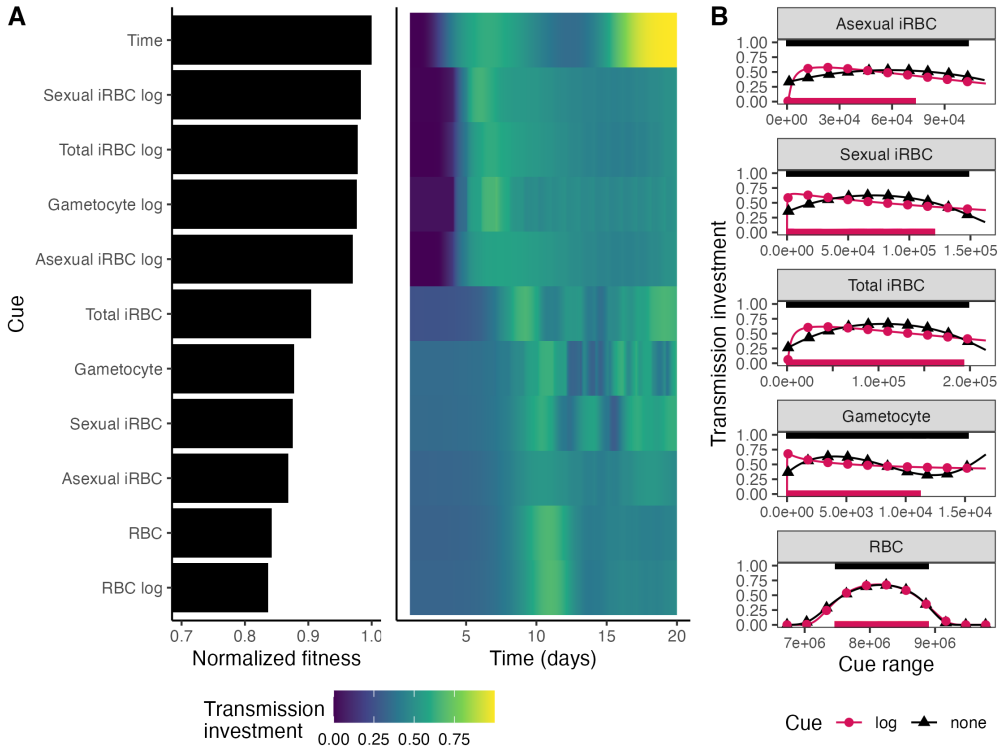

Fig 2. Cue perception mediates parasite transmission investment dynamics. (A) On the left, fitness values achieved by parasites adopting the optimal transmission investment strategy for each cue, normalized with respect to the time-varying strategy, are displayed in descending order. On the right, the dynamics of transmission investment, given the optimal reaction norms, are plotted. Of all parasites sensing only one cue, sensing parasite densities on a $\log_{10}$ scale enables parasites to obtain the highest fitness, and produces an early delay in transmission investment. (B) Optimal reaction norms for different cues. Each facet displays the reaction norms for raw (black triangle) or log-transformed (red circle) cues. The ranges of cue values "experienced" by a parasite adopting the optimal reaction norm are displayed above (raw) or below (log-transformed) the reaction norms as rug plots. Based on the shape of the reaction norms, we conclude that sensing log-transformed parasite-centric cues enables more sensitive detection of (and responses to) early rises in parasite abundance.

Dual cue perception is necessary for terminal investment

Given that single cue perception fails to recapitulate the patterns of transmission investment obtained when investment is a function of time, specifically terminal investment, we next examined whether perceiving two cues simultaneously could. Put simply, many within-host cues go up and then down, or vice versa, over the course of an infection, so a single cue cannot uniquely identify "where" (or when) in an infection a parasite is, e.g., whether conditions are good and parasites are proliferating (iRBC density is low), or conditions are bad and the infection is nearing its end (iRBC density is also low). Integrating two cues should provide hysteresis or a unique state for each infection stages, allowing for more control of transmission investment in late infection.

We evaluated the fitness of parasites sensing all pairwise combinations of cues using numerical optimization of spline surfaces. Our results suggest that sensing most dual

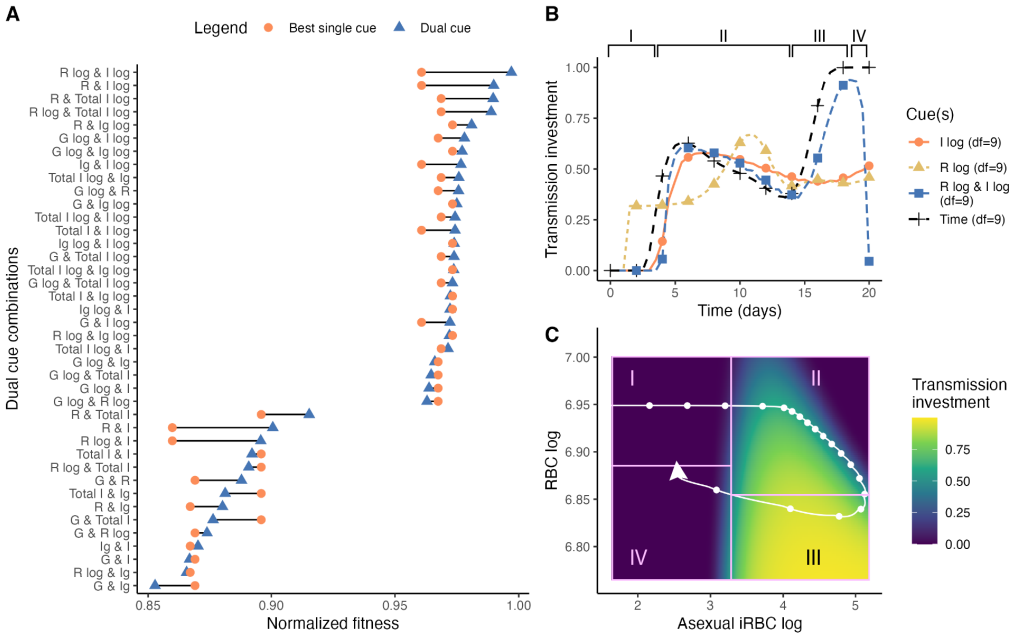

Fig 3. Dual cue perception increases parasite fitness and enables terminal investment. (A) The fitness of parasites (normalized with respect to the time-varying strategy) adopting the optimal strategy for each dual cue combination is indicated with a blue triangle, while the fitness obtained when perceiving the best performing single cue (of the combination) is represented with an orange circle. To obtain the fitness of a fair comparator time-varying strategy, we optimized transmission investment as a function of time using a spline with nine degrees of freedom (the same degrees of freedom used in the dual cue model), rather than the three degrees of freedom used above and in previous work [20]. (Note that previous work showed the marginal fitness gains of using more flexible splines were small [20], but tracking two environmental cues necessitates more degrees of freedom.) (B) The pattern of transmission investment over time for parasites sensing the best dual cue combination (R log & I log, blue square) along with individual components of the cue (I log, orange circle; R log, yellow triangle; each optimized with nine degrees of freedom) and the ideal dynamic (Time, black cross) are plotted together. Parasites sensing logged asexual iRBC and logged RBC engage in late-infection terminal investment. (C) Transmission investment (colour of heatmap) is plotted as a two-dimensional reaction norm, with logged RBC and logged asexual iRBC as cues. The white line indicates the trajectory of infection for parasites adopting this optimal reaction norm strategy, with each point on the line representing a single day. The arrow on the white line indicates the passage of time. For (B-C), the four stages outlined in the results section are annotated with I, II, III, and IV.

cue combinations improves parasite fitness relative to sensing a single cue (Fig 3A), with parasites sensing raw/logged RBC and logged iRBC (asexual or total) exhibiting notably higher fitness (Fig 3A). This higher fitness is conferred by transmission investment patterns that are close to the time-varying ideal, with an initial delay in transmission investment and a late infection (nearly) "terminal" investment before returning to a low transmission investment (Fig 3B, S2 Fig). Increasing the spline flexibility of the single cue models could not reproduce this same pattern (Fig 3B), confirming that dual cue perception specifically enables terminal investment. Although the biggest gains in fitness accrue for strategies that permit an initial delay (S3 Fig), parasites that engage in terminal investment accrue higher fitness near the end of

infection (day 18 onward) relative to parasites that do not (S3 Fig).

To better understand how the pattern of transmission investment changes over the course of an infection, we next analyzed the reaction norm of the dual cue combination that conferred the highest fitness: logged asexual iRBC and logged RBC. The pattern of transmission investment is defined by a looping journey through the reaction norm surface (Fig 3C), confirming that the cue combination traces a unique path over the course of an infection (i.e., a hysteretic relationship [34]). We categorized the reaction norm into four distinct sections/stages (Fig 3C). Stage I corresponds to the initial phase of infection, characterized by low transmission investment, low parasite density, and high RBC density (Fig 3B-C). As the infection progresses, the reaction norm enters stage II, characterized by asexual iRBC production and RBC decline. During this stage, the optimal transmission investment increases considerably, followed by subtle declines as the iRBC population continues to increase (Fig 3B-C). This transition from a low to high transmission investment observed as stage I transitions into stage II constitutes delayed transmission investment. Following peak parasite density, the reaction norm enters stage III, which is marked by decreasing iRBC population and gradual replenishment of RBC, signaling imminent infection clearance. At this stage, transmission investment increases to peak levels (i.e., terminal investment). Finally, as the infection nears clearance and the reaction norm enters stage IV, transmission investment sharply drops as the host heads towards recovery (Fig 3B-C). We note that this drop in predicted transmission investment is likely a consequence of the constraints of the spline surface, and different strategies during this stage would have negligible impact on fitness. (We also note that some dual cue combinations exhibit sustained terminal investment through this final stage; S2 Fig). Overall, our results suggest that each cue plays a crucial role in defining progression through infection stages I to III, with asexual iRBC density exhibiting the largest variation in early and late infection (stages I and III), and logged RBC density exhibiting the largest variation during mid-infection (Stage II; Fig 3C). This temporal staggering of iRBC and RBC dynamics ensures that these infection stages can be tracked. As a result, dual cue perception provides parasites with the ability to "state differentiate," to accurately monitor the progress of the infection and adjust transmission investment accordingly.

Intriguingly, the dual cue combinations that are most informative for parasites making life history decisions (top five in Fig 3A) are also the most informative for predicting patient outcomes in clinical malaria infections [34]. In both cases, two slightly out-of-phase within-host measures can uniquely define a patient's (or simulated host's) position on the path from health through sickness to recovery. Plotting this trajectory through disease maps (i.e., the two measures plotted against each other, as in Fig 3C) produces a looping, or hysteretic, pattern, with each infection stage occupying a unique coordinate in this two-dimensional space [34]. To further validate that forming the characteristic looping pattern is a unique feature of our identified best cue combinations, we constructed disease maps using experimental data from laboratory mice infected by a single strain of *P. chabaudi* [12, 30–33] and simulated data from our dual cue models. Both experimental and simulated data indicate that raw or logged RBC with logged iRBC (asexual or total in the model; only total is available in the data) are the only cue combinations that generate loops (e.g., Fig 4A and B), while other cue combinations do not (e.g., Fig 4C and D; full data shown in S4 Fig and S5 Fig). We note that disease maps generated with RBC and logged gametocyte density are flattened during parasite clearance (S4 Fig) as a result of the longer sexual development period, which may explain why parasites sensing this dual combination do not display terminal investment. In summary, our results demonstrate that terminal

investment requires parasites to unambiguously state differentiate, track infection stages, and dynamically adjust transmission investment in response to changing conditions. Our data suggests that perceiving hysteretic cues — of which a combination of RBC and logged iRBC provides a clean delineation of different infection stages — is a viable method of attaining state differentiation.

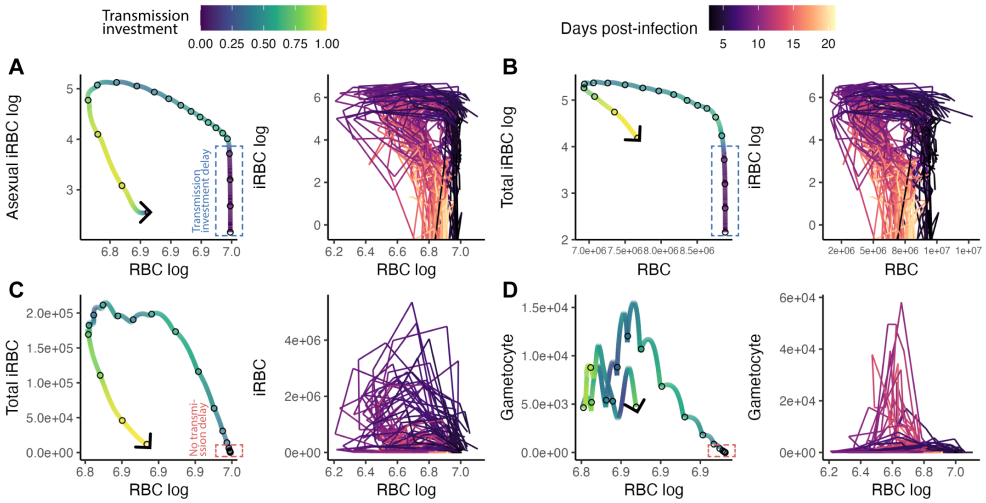

Fig 4. Trajectories of RBC and log-transformed iRBC densities form a looping pattern *in silico* and *in vivo*. Simulated (left) and experimental (right) trajectories of cues that (A-B) enable transmission delay and terminal investment or (C-D) do not enable an adaptive transmission investment strategy. For each panel, the left graph displays the results from our simulations, with the distance between each circle representing a single day and the colour of the line the observed transmission investment. The right graph displays the infection trajectory of laboratory *P. chabaudi* infections in mice. The colour of the lines indicates the number of days post-infection. Note that asexually- and sexually-committed iRBCs could not be distinguished in the experimental data. For the simulated trajectories, the first 3 days (corresponding to the period of delayed transmission investment) is outlined by a blue, dotted box. As can be seen in (C-D), early changes in the environment cannot be clearly delineated based on unlogged abundances (see the red, dotted box), therefore preventing a delayed transmission investment strategy. Additionally, separation of early and infection trajectory allows for both early transmission delay and terminal investment.

Dual cue perception exacerbates the fitness loss incurred by environmental stochasticity

The benefits of plasticity depends on the quality of the information organisms obtain from environmental cues. Adaptive phenotypic plasticity is contingent on proper phenotype–environment matching, where the perceived cue is a reliable predictor of the optimal phenotype [35–39]. Theory suggests that a weak correlation between cue(s) and the optimal phenotype (i.e., low cue reliability) could disfavour plasticity relative to other strategies (i.e., local adaptation [36, 37, 40], canalization [39], bet-hedging [40]). One way that low cue reliability emerges is through environmental stochasticity. Although our model allows parasites to sense components of their state, and their resulting level of transmission investment will feedback to influence that state, the results above assume that all else is equal between hosts (i.e., the optimal reaction

norms identified are associated with a specific set of model parameters). For malaria parasites, variation in host characteristics (e.g., RBC availability [41–43], immunity [43–46]) and parasite development (e.g., burst size variation [43]) could alter the fitness consequences of our putative optimal strategies and could change optimal reaction norms, making partial phenotype-environment matching inevitable. The ability of a reaction norm to maintain parasite fitness given environmental stochasticity is thus vital for the evolutionary maintenance of plasticity [39, 47]. To investigate how biologically relevant variation affects cue performance, we built a semi-stochastic model based on the work of Kamiya *et al.* [43], which employed a hierarchical Bayesian method to quantify inter-host variation in parasite burst size, erythropoiesis (RBC replenishment), and immune strengths. We note that the variation observed in natural infections is likely to be considerably higher, given numerous sources of heterogeneity compared to the dataset fitted by Kamiya *et al.* that includes only a single mouse host genetic background studied in a highly controlled experimental system [24]. Hence, the inter-host/environmental variation we include will likely underestimate the penalties incurred by environment-phenotype mismatching but should, nevertheless, provide valuable insights into how biological variation influences the evolution of transmission investment.

We first sought to understand how environmental variation affects the fitness of parasites adopting strategies optimized under deterministic conditions (i.e., with invariant model parameters). For all single cues and the top four performing dual cues, we performed 1000 20-day simulations and simultaneously varied the RBC replenishment rate (ρ), parasite burst size (β), immune activation strengths (ψ_n and ψ_w) and immunity half-lives (ϕ_n and ϕ_w), sampling parameter values from the posterior distributions previously reported [43] (S6 Fig). Each choice of parameter set will influence the within-host infection dynamics, potentially altering the trajectory of the perceived cue(s), resulting in different, expressed patterns of transmission investment and, thus, fitness. We quantified the effect of this variation on cue performance using the geometric mean fitness, which is commonly used to assess fitness in fluctuating environments [48, 49]. We find that the geometric mean fitness of parasites responding to a given cue, in the face of this environmental variation is largely uncoupled from fitness in the deterministic model (i.e., the environment in which the strategy was optimized; Fig 5A), emphasizing that the "best" reaction norm for a certain condition does not always confer the best phenotype in another environment. Interestingly, three out of the four dual cues have a lower geometric mean fitness than the best-performing single cues (Fig 5A), indicating a potential tradeoff between fine-tuning fitness in a given environment and susceptibility towards environmental stochasticity.

To determine the dominant contributors to the observed variation in fitness, we repeated the simulations, but allowed only one parameter to vary. For all cues, variation in burst size exerted the largest influence on fitness (Fig 5B) with a median relative fitness perturbation of $\sim$1, meaning that perturbing burst size alone leads to a fitness decline similar in magnitude to perturbing all six parameters. Our finding is in agreement with prior literature on the importance of burst size for parasite transmission [50]. For certain cues, variation in indiscriminate immunity (half-life and activation energy) and the activation energy of targeted immunity also contribute to losses in fitness (Fig 5B). We note that the susceptibility of cues towards variation in specific parameters is sometimes related to the "proximity" of the parameter to the cue, e.g., parasites sensing RBC density are more susceptible to variation in indiscriminate immunity that depletes RBC (ψ_n, ϕ_n) and RBC replenishment rate (ρ; Fig 5B). Dual cue sensing parasites "inherit" this increased susceptibility toward certain parameter

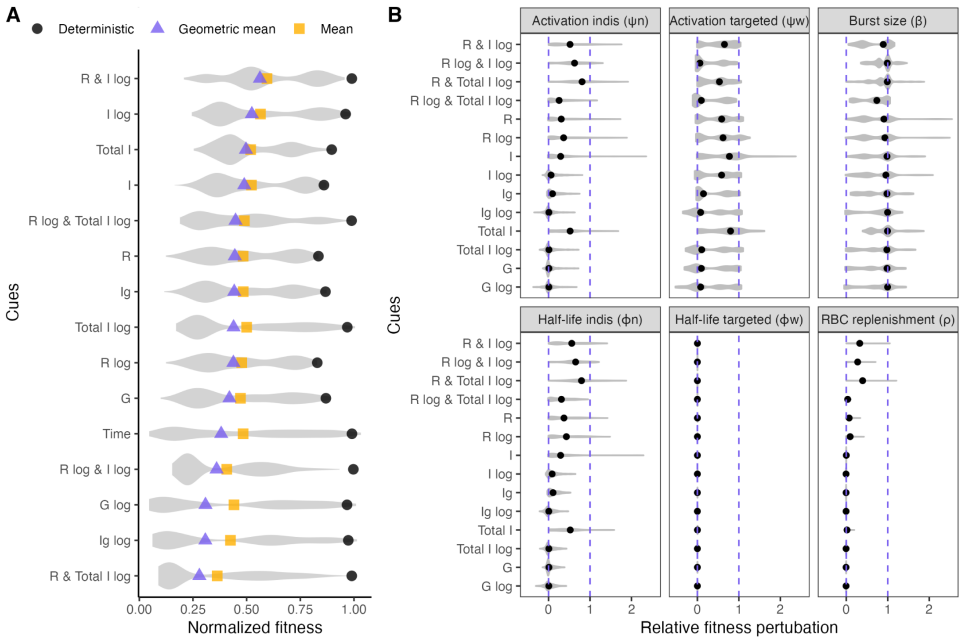

Fig 5. Optimal transmission investment under certain conditions does not always translate effectively across different environmental and developmental variations. (A) Fitness of parasite strategies in the deterministic model is largely uncoupled from their geometric fitness in the full semi-stochastic model. We performed 1000 20 days simulations of parasites adopting the optimal transmission investment strategy (from the deterministic model) using a semi-stochastic model where six parameters are randomly drawn from the posterior distributions derived by Kamiya *et al.* [43]. The distribution of fitness values is represented by a grey violin plot while the summary statistics (fitness from the deterministic model, geometric mean fitness, mean fitness) are represented with a black circle, purple triangle, and yellow square, respectively. The fitness values are normalized with respect to the fitness of the time-varying strategy with nine degrees of freedom. (B) Variation in burst size and immune strengths contribute most to fitness loss. To determine the contribution of individual parameters, we repeated the simulations with only one parameter varying. The relative contribution of each varied parameter (indicated by the facet label) is quantified by the ratio between the fitness difference with one parameter varying ($\text{fitness}_{\text{single}} - \text{fitness}_{\text{det}}$) and the fitness difference with all six parameters varying ($\text{fitness}_{\text{all}} - \text{fitness}_{\text{det}}$). Here, the relevant range of the ratio is between 0 and 1 (negative ratios or ratios > 1 are produced when the fitness obtained from the semi-stochastic model is larger than the deterministic model fitness, which is rare). A relative fitness perturbation near 0 suggests that the parameter perturbed contributes very little to the fitness decline, while a ratio near 1 suggests the opposite. The distribution of relative fitness perturbation within the 89% credible interval (highest posterior density interval) is displayed by a grey violin plot. The median of the distribution is represented by a black circle.

variations associated with perceiving RBC density. For example, when simulations are performed with variation in indiscriminate immunity activation strength or half-life, the top four dual cue sensing strategies, which all include RBCs or logged RBCs as a cue, experience large fitness declines (S7 Fig). Thus, while dual cue perception facilitates state differentiation and fine-tuning to the environment, it can make parasites more

susceptible to cue variations and exacerbate phenotype-environment mismatching.

We next explored why certain cues are more sensitive to parameter perturbations. To simplify, we envisioned a fitness landscape where the y-axis represents the total transmission potential accrued during an acute infection, and the x-axis represents an arbitrary transmission investment strategy. For any given parameter perturbation, changes to the fitness landscape are expected to shift the optimal transmission investment strategy (Fig 6A). Depending on the cue, such perturbations may have varying impacts. In some cases, parameter changes may minimally affect cue values throughout an infection, enabling parasites to maintain a consistent pattern of transmission investment (see "No change" in Fig 6A). Although the pattern remains similar, the fitness payoff may differ based on the newly shifted optimal investment reaction norm. In contrast, parameter changes may significantly alter cue values, leading to changes in the expressed transmission investment pattern. These changes can be adaptive, improving fitness, or non-adaptive, resulting in fitness declines (Fig 6A). Adaptive changes are characterized by a positive correlation between fitness and the degree of change in transmission investment, whereas non-adaptive changes exhibit the opposite trend (Fig 6A). To distinguish between these scenarios, we examined the relationship between shifts in transmission investment strategy (quantified as the median absolute difference in transmission investment over time relative to the deterministic model) and fitness changes (calculated as the geometric mean fitness across simulations minus the fitness of the deterministic model). Our analysis revealed that for most parameters, cues associated with the largest fitness reductions also exhibited the greatest changes in transmission investment (Fig 6D). This pattern suggests that parasites are non-adaptively altering their transmission investment in response to environmental variability. This relationship becomes evident when comparing the transmission investment dynamics of a cue not susceptible to parameter perturbations (e.g., logged asexual parasite density; Fig 6B) with a susceptible dual cue (e.g., RBC and logged total iRBC; Fig 6C). The latter shows much greater variability in transmission investment patterns, particularly during the early stages of investment, where significant fitness gains or losses are most likely to occur.

Interestingly, we note that the pattern of delaying investment at the start of infections is surprisingly robust to environmental perturbation. This robustness is likely due to the relative simplicity of detecting a large, multi-log-fold change in population density early in infection compared to sensing smaller magnitude changes later in the infection stages. Overall, we conclude that environmental stochasticity can lead to fitness loss by causing parasites to"deviate" from their original transmission investment strategy (i.e., non-adaptive changes to transmission investment).

Dual cue perception leads to higher virulence

Given that cue perception mediates infection dynamics, it could also influence the severity of infections, or virulence. We estimated virulence using the methods described in Torres *et al.* [34], where infection dynamics are mapped in disease space, with the y-axis quantifying host health (RBC density) and the x-axis quantifying parasite load (total iRBC density). A more virulent infection is expected to produce a higher parasite load while consuming more host resources, tracing a larger loop through disease space. To evaluate the effects of cue perception on virulence, we generated 30-day disease maps of infections, allowing sufficient time for the infection to fully resolve in our model. We use the area enclosed by each disease map as a proxy for virulence, with larger areas indicating higher virulence.

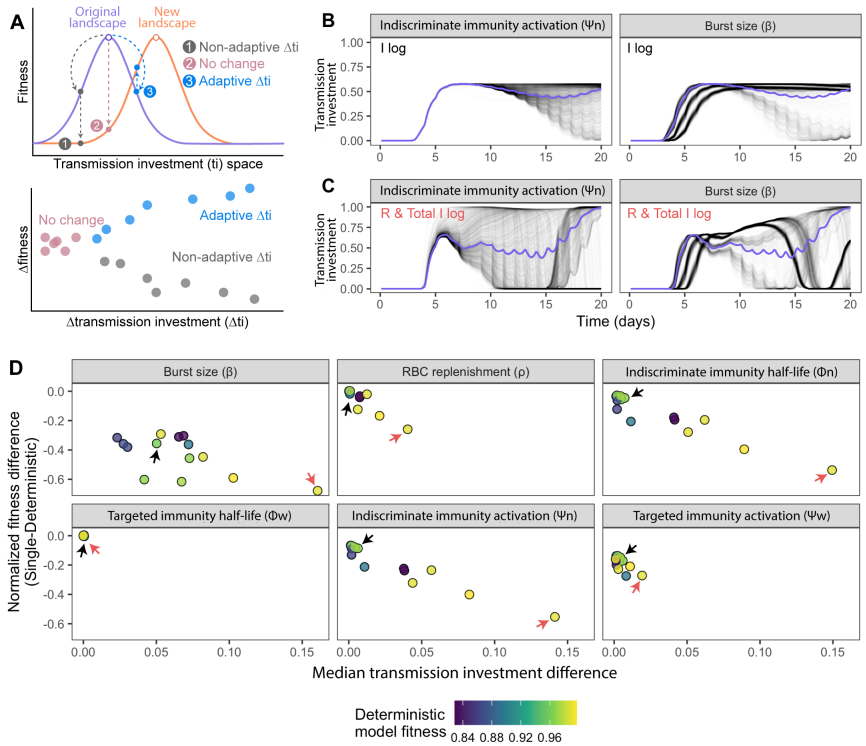

Fig 6. Variation in patterns of transmission investment underlies cue susceptibility to parameter variation. (A) Environmental stochasticity can result in phenotype–environment mismatches, leading to fitness loss. The top panel illustrates changes in the fitness landscape due to environmental variability. The purple curve represents the original fitness landscape to which the organism is adapted ("optimized"), while the orange curve shows the altered fitness landscape resulting from environmental changes. In response to stochasticity, an organism may maintain its original trait value (option 2, plum), resulting in lower fitness in the new environment. Alternatively, the trait value may be modified either in a non-adaptive (option 1, grey) or adaptive manner (option 3, blue). The bottom panel depicts the hypothetical relationship between changes in the expressed pattern of transmission investment due to altered cue trajectories (x-axis) and fitness change (y-axis) under these three scenarios. (B-C) Each facet shows the transmission investment dynamics of parasites adopting the optimal reaction norms from the deterministic model, but in an environment with randomly sampled parameter values for indiscriminate immune activation energy (left panel) or burst size (right panel). A parasite sensing logged asexual iRBC displays less variation in transmission investment dynamics (B) compared to a parasite sensing RBC and logged total iRBC (C) in the face of environmental stochasticity. (D) Each facet presents the relationship between changes in transmission investment dynamics (x-axis) and fitness loss (y-axis; where the fitness values are normalized with respect to the time-varying strategy) when only one parameter is altered. In general, parasites with greater changes in transmission investment suffer larger fitness losses, suggesting that parasites are non-adaptively altering their transmission investment strategy. The positions of parasites sensing logged asexual iRBC (a robust cue) or RBC and total logged iRBC (a cue susceptible to parameter variations) are indicated by black and red arrows, respectively.

We find that parasites perceiving only a single cue trace smaller disease maps than parasites that adopt the ideal pattern of transmission investment (by sensing time; Fig 7A). Additionally, the area of the disease map is negatively correlated with parasite fitness across all single cues (Fig 7B), suggesting that if parasites are constrained to perceive a single cue, strategies that result in lower virulence might be favoured. Parasites sensing the top four dual cue combinations produce disease maps that are similar to the map traced by parasites adopting the time-varying strategy (Fig 7C) and, in general, display higher virulence relative to parasites sensing a single cue (Fig 7D; compare x-axis values of points in B and D). Overall, these findings suggest that if parasites have limited information (single cue perception), virulence will be lower, while if parasites are capable of more finely tracking infection stages through dual cue perception, they will exploit host resources to a greater extent and therefore be more virulent.

Discussion

Just as with any sexually-reproducing species, investing in reproduction by producing gametocytes is critical for the fitness of *Plasmodium* spp., as this is the only parasite stage capable of being transmitted to mosquito vectors. As for other species, this investment comes with tradeoffs for malaria parasites: a given infected host cell can either produce multiple asexual progeny that can infect new host cells and have the potential to grow or maintain a given infection, or a single, sexually-differentiated gametocyte with the potential to "reproduce" an infection [51]. Thus, maximizing parasite fitness requires balancing these competing demands, the relative importance of which is likely to shift over the course of infection, as the within-host environment changes in response to parasites exploiting the host. Indeed, data show that transmission investment varies throughout infections [12–14] and appears to change in response to drug treatment [52] in ways predicted to be beneficial for parasites (e.g., [27, 52]). While adaptive plasticity is a well-known solution to the challenge of living in a changing environment (e.g., [53]), there has been skepticism about the fitness benefits of observed parasite plasticity [54], in part because knowledge of parasite environmental sensing mechanisms remains limited. Previous mathematical modeling has treated parasites as either insensitive to environmental change (i.e., constant transmission investment [18, 19, 21–23, 55–57]) or as perfectly informed (time-varying investment [20, 29]). We instead ask what environmental cues malaria parasites *should* use to set transmission investment, demonstrating that no single cue allows parasites to achieve the best time-varying strategy [20]. Parasites must sense two cues to recapitulate the optimal strategy but that strategy enhances the risk of parasites being "tricked" by environmental and developmental stochasticity into expressing suboptimal phenotypes. We further show that if parasites have the capacity to sense more aspects of their within-host environment, then this has negative consequences for host health.

Previous theoretical work identifies two key features of optimal transmission investment strategies for *P. chabaudi* [20]. First, there should be no investment at the start of infections, when densities are too low to permit successful infection of vectors (i.e., transmission delay). Second, parasites should invest all resources into transmission just before an infection ends, a "terminal investment" strategy from life history theory [10]. Our results delineate the environmental cues that can recapitulate these features. Transmission delay requires a sharp, threshold-dependent transition from "no transmission" to an intermediate transmission state as the parasite population grows. Making clear-cut decisions in response to continuous cues are common in biological

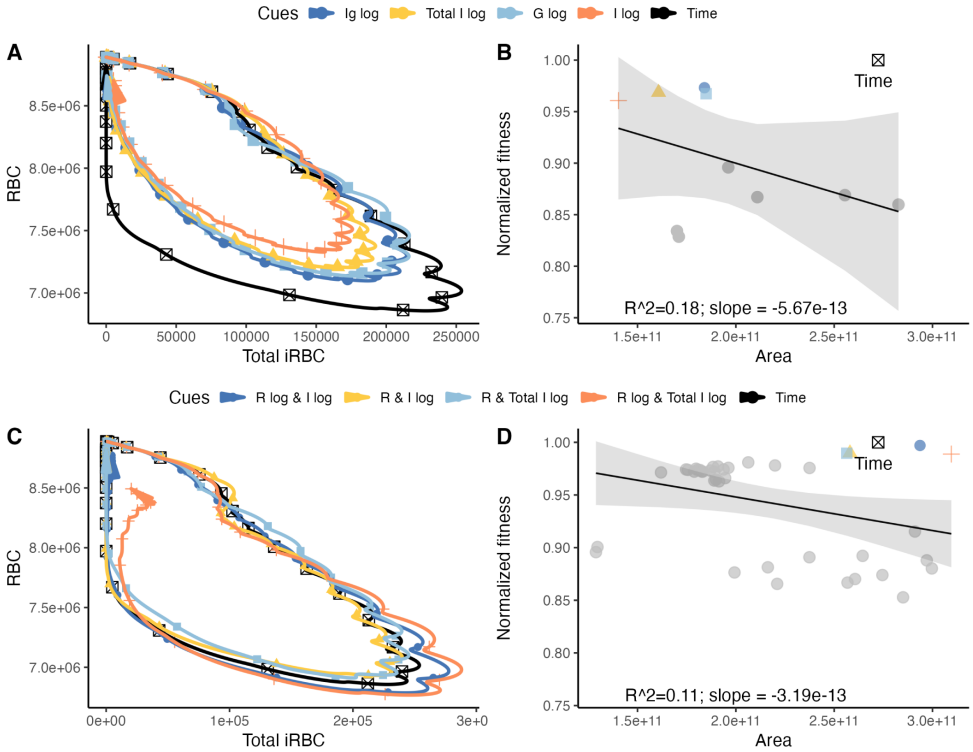

Fig 7. Cue perception mediates parasite virulence. (A, C) display the 30-day disease maps of infections where parasites adopt the top four optimal transmission investment strategies when sensing (A) a single cue or (C) dual cues. We use the area of the map traced as a proxy for virulence [34]. The trajectory of parasites that adopt the ideal transmission investment strategy (sensing time) is shown in black. (B, D) Relationship between disease map area and fitness (normalized with respect to the time-varying strategy) for parasites that sense (B) only one cue or (D) dual cues. The top 4 cues for single or dual cue perceiving parasites are coloured. The linear regression prediction with 95% confidence interval and R^2 values are shown. Note that the values for parasites adopting the optimal time-varying transmission investment ("Time") are shown for reference and are not included in the linear regression analysis. Overall, these results show that perceiving only a single cue could generate selection for strategies that lead to lower virulence and that perceiving two cues increases virulence relative to a single cue.

systems (e.g., cell cycle commitment [58] and developmental patterning [59]) and often relies on ultrasensitivity characterized by a steep response curve. Our results demonstrate that having an ultrasensitive reaction norm where transmission investment rises sharply after a certain population threshold— a characteristic enabled by sensing parasite-centric cues on a logarithmic scale—is sufficient for transmission delay. Interestingly, although RBC availability has been shown experimentally to affect transmission investment [14, 29], our findings indicate that sensing RBC density only is insufficient for producing an early delay in investment. This is likely due to the fact that RBC densities change very little early on in infection and overall span a range within a single order of magnitude (while parasite densities span several orders of magnitude within the first week of these experimental infections). Consequently, RBC density alone cannot provide an adequate signal for early-stage decision-making.

Our results also suggest that parasites perceiving a single cue do not exhibit terminal investment, possibly due to their inability to distinguish between different infection stages or "states". Since most within-host environmental variables go up and down, or vice versa, over time (e.g., parasite densities rise and then fall due to resource limitation or immunity; resources decline due to parasite exploitation and then are replenished), one cue cannot provide enough detail to unambiguously establish "where" a parasite is in the course of infection. In line with this logic, researchers seeking to define a host's trajectory over time from health through sickness and on to recovery [60] found a combination of two within-host measures (e.g., parasite density and resource abundance) that are slightly out of phase with each other and can uniquely determine a patient's position on their path for malaria infection (i.e., are hysteretic) [34]. Similarly, we find that parasites sensing a combination of logged iRBC (a measurement of parasite density) and RBC (logged or not logged; a proxy for resource abundance) can engage in terminal investment and that each stage of infection can be characterized by a unique combination of these cues. Our results thus demonstrate that perceiving RBC, while not necessary for transmission investment delay, can enable terminal investment. Additionally, the information desired by medical professionals seeking to predict patient outcomes is also the most informative for parasite life history decisions.

Theory demonstrates that terminal investment is an adaptive strategy for malaria parasites, given perfect information about when infections will end [20]. However, experimental studies of *P. chabaudi* suggest a modest increase in transmission investment at infection resolution [61] or in response to antimalarial exposure [52]. In *P. falciparum*, a high transmission investment ($\sim$70%) is obtained only when parasites are exposed to highly artificial conditions (e.g., extreme crowding or choline-free media to mimic a lack of gametocyte production-stimulating lysoPC (lysophosphatidylcholine) [62, 63]). What underlies the discrepancy between theoretical predictions and empirical observation? Part of it may stem from the difficulty of accurately quantifying transmission investment [15]. Past theory also suggests that variation in infection length can select against terminal investment, since the benefits are outweighed by the costs of continuing to transmit from longer infections [20]. Our study also reveals a potential evolutionary explanation through the tradeoff between robustness and fitness in a given environment. Dual cue-sensing parasites, while capable of terminal investment, are more sensitive to variations in environmental parameters and experience large fitness declines when the simulated condition deviates from the conditions in which their transmission investment strategy is optimized. Thus, terminal investment may be risky even when infection length is consistent, due to variability in environmental cues across hosts. Additionally, the fitness benefit gained from terminal investment is small relative to that accrued by delaying early transmission investment (as was also seen in [20]), consequently the fitness difference between the dual cue models and the best single cue model is also small. Therefore, this increased sensitivity to environmental perturbation and small fitness advantage of engaging in terminal investment may explain the lack of evidence for terminal investment.

The tradeoff hypothesis for virulence evolution stipulates that pathogen transmission inevitably harms the host [64]. While the generality of this framework has been contested (see [65] and references within), empirical data from *Plasmodium* spp. have generally supported a positive relationship between parasite virulence and transmissibility [66–69]. Previous work has shown that host heterogeneity can constrain parasite virulence evolution [70–72]. Here, we demonstrate that if parasites are limited to sense a single cue, then the optimal transmission investment strategies (and the associated reaction norm for each cue) result in less host exploitation. In fact, the most

fit single cue strategies result in lower virulence than when parasites have access to more than one cue or perfect information. Yet, our results suggest that responding to more than one cue can render parasites more susceptible to non-adaptive transmission strategies in the face of environmental noise within the host. Thus, the need for parasites to balance state differentiation with the cost of sensing noisy signal may be another mechanism by which variability across hosts can constrain virulence evolution.

Mathematical modeling has enabled us to explore the fitness consequences of cue perception in *P. chabaudi*, and our results suggest where greater model complexity would be most or least informative. For example, incorporating variation in gametocyte circulation time [13] would further undercut the reliability of gametocytes as a cue. We note that *P. falciparum* has a longer sexual development period of 9-12 days [73] and this longer lag between cue perception and phenotype expression will reduce cue reliability [74]. Thus, we anticipate the value of sensing sexual parasite-centric cues to decrease even further in this species and believe our finding that gametocyte abundance is a poor cue is likely to be robust. While we have ignored parasite developmental processes that occur in the vector, recent theory suggests they have little qualitative impact on optimal transmission investment strategies [75]. In contrast, the impact of previous exposure on host immunity represents one area where more complexity could qualitatively alter predictions. Our models also depict immunologically naive hosts, but where malaria is endemic, parasites will often find themselves in a host with a prior history of infection. Understanding how immune memory influences the quality and reliability of potential within-host cues represents an important area for future research. Our selection of cues assumes that parasites sense only the magnitude of a cue, without detecting temporal changes in that magnitude. However, evidence from other systems (e.g., bacterial chemotaxis [76] and yeast responses to nutrient limitation [77]) suggests that organisms can perceive relative changes in cues rather than absolute levels. This ability to detect changes over time may provide more relevant information for decision-making. Nonetheless, we anticipate that the key features of a "useful" cue—ultrasensitivity to low population density changes and hysteresis—will broadly apply, regardless of the specific nature of the cue. Another important model assumption is that all parasites perceive the same cue at the same strength, but cues may not be spatially uniform. Variation in signal strength and imperfect cue sensing could lead to heterogeneity in transmission investment in a genotypically uniform parasite population, similar to the dynamics observed in bacterial biofilms [78]. Extrapolating from our results, we hypothesize that if the variation in signal strength is large enough, selection may favor single cue sensing due to the relative robustness to stochastic variation.

Beyond malaria, our findings add support to theory suggesting that the adaptive benefits of phenotypic plasticity are enhanced when cues enable organisms to sense distinct states that correspond to specific optimal phenotypes [79] and when organisms perceive cues that are robust against environmental fluctuations [39, 80]. Yet counterintuitively, we show that these two benefits of plasticity can trade off, such that perceiving more cues allows organisms to better approximate optimal strategies while rendering them more susceptible to stochastic environmental and developmental change. Such tradeoffs may represent important constraints both on the evolution of sensing systems and on the evolution of plastic reproductive investment strategies.

Materials and methods

Within-host model of *P. chabaudi* infection dynamics

We modified and extended a previously published mathematical model describing the within-host infection dynamics of the rodent malaria parasite, *P. chabaudi* [20] (Fig 1). The original model consists of ordinary and delay differential equations representing the interactions between the parasite, host red blood cells (RBCs), and host immunity over a 20-day infection period. While the original model defined transmission investment as a function of time, we modeled transmission investment as a function of cue(s) to better capture the mechanism of phenotypic plasticity, since there is no evidence malaria parasites track time across multiple generations. Furthermore, we revised the model to reflect the Next Cycle Conversion (NCC) phenomenon. Previous studies found that sexually-committed parasites in *P. falciparum* canonically do not engage in gametocytogenesis until the next infection cycle [26]. To account for NCC dynamics, our model assumes that infected RBCs commit to producing either sexual merozoites (M_{g}) or asexual merozoites (M) at the beginning of their maturation cycle. Gametogenesis occurs when a sexually-committed merozoite invades a susceptible RBC, effectively introducing a delay between sexual commitment and the outcome of sexual commitment (i.e., production of an infected RBC (iRBC) that will produce a gametocyte, I_{g}). Additionally, based on the findings of Kamiya *et al.* [43], we incorporated two forms of immunity into our model—a targeted immune response that only kills iRBCs and an indiscriminate response that kills any RBC —to better capture host defense mechanisms.

We parameterized our model based on prior works on malaria intrahost dynamics [20, 43] (Table 2). Because parameter values in Kamiya *et al.* [43] depend on initial dosage (I_0), we estimated our starting dose using the same method, which corresponds to approximately 10^4-10^5 iRBCs. Preliminary investigations indicate that varying the initial iRBC dosage did not lead to quantitative differences in parasite relative fitness. Consequently, we parameterized $\psi_n, \psi_w, \phi_n, \phi_w$ and ρ using the median posterior estimates assuming an initial dosage of 10^4 iRBCs.

Table 2. Parameter values used in the intrahost *P. chabaudi* model.

Parameter	Definition	Value	Unit	Source
R_0	Equilibrium RBC concentration	$8.89 * 10^6$	RBC/μL	[24]
μ	Background RBC/iRBC mortality rate	0.025	day^{-1}	[45]
p	Infection probability of RBC by merozoite invasion	$8 * 10^{-6}$	day^{-1}	[81]
α	Asexual iRBC development period	1	day	[82]
α_g	Sexual iRBC development period	2	day	[83]
β	Burst size; number of merozoites produced per iRBC	5.721	merozoites	[84]
μ_m	Background merozoite mortality rate	48	day^{-1}	[81]
μ_g	Background gametocyte mortality rate	4	day^{-1}	[83]
I_0	Initial iRBC inoculum size	43.85965	iRBC/μL	[20]
sp	Shape parameter dictating iRBC synchrony	1	NA	[85]
ψ_n	Activation strength for indiscriminate immunity	16.69234	NA	[43]
ψ_w	Activation strength for targeted immunity	0.8431785	NA	[43]
ϕ_n	Half-life of indiscriminate immunity	0.03520591	day	[43]
ϕ_w	Half-life of targeted immunity	550.842	day	[43]
ι	Minimum iRBC concentration to induce maximum immunity	$2.18 * 10^6$	RBC/μL	[24]
ρ	Maximum proportion of RBC recovered per day	0.2627156	NA	[43]

Our model mimics the infection dynamics of experimental *P. chabaudi* infections in mice. At the onset of the infection, the host receives an initial dose of asexually-committed iRBC (I_0). We assume no parasites in this initial dose commit to gametocytogenesis and all produce asexual merozoites (M). Therefore, before the end of the first asexual development period ($t \leq \alpha$, where α is the development period of one day for this species), the dynamics of asexual iRBC (I) in the host are determined solely by the invasion of RBC by asexual merozoites, natural RBC death, maturation of the initial cohort of infected cells, and immune-mediated killing such that

$$\frac{dI}{dt} = \underbrace{\epsilon R(t)M(t)}_{\text{RBC invasion}} - \underbrace{\mu I(t)}_{\text{Natural death}} - \underbrace{I_0 Beta(sp, sp)S}_{\text{iRBC maturation}} - \underbrace{[-ln(1 - N(t)) - ln(1 - W(t))]I(t)}_{\text{Indiscriminate and targeted immunity}}. \quad (1)$$

$\epsilon R(t)M(t)$ represents the production of iRBC through asexual merozoite invasion of RBCs, which occurs at a rate of ϵ per day, given contact. Infected RBCs die at a background rate of μ, while $-ln(1 - N(t))$ and $-ln(1 - W(t))$ describe their rate of death due to indiscriminate and targeted immunity, respectively. The infection-age structure of the initial cohort of asexual iRBCs, denoted as $Beta(sp, sp)$, is modeled using a Beta distribution with a shape parameter $sp = 1$, allowing iRBC maturation to occur with a uniform probability throughout the development period [85]. The uniform probability of maturation for the initial cohort is computationally efficient and provided extremely similar results to more narrow age distributions in a previous modeling study [20]. The rate of asexual iRBC maturation depends on an exponential survival function S, which describes the proportion of iRBC that survives until maturation. S is defined by a cumulative hazard function that is calculated by integrating the total rate of death across the development period:

$$S = exp[-\int_{t-\alpha}^{t} \underbrace{\mu}_{\text{Natural death}} \underbrace{-ln(1 - N(\omega)) - ln(1 - W(\omega))}_{\text{Indiscriminate and targeted immunity}} d\omega]. \quad (2)$$

During the period $t \leq \alpha$, asexual merozoite production is described by

$$\frac{dM}{dt} = \underbrace{\beta I_0 Beta(sp, sp)S}_{\text{iRBC maturation}} - \underbrace{\mu_m M(t)}_{\text{Natural death}} - \underbrace{\epsilon R(t)M(t)}_{\text{RBC invasion}}, \quad (3)$$

where the first term represents the production of asexually-committed merozoites by asexual iRBC that have survived the duration of the developmental cycle and burst to produce β merozoites each. Asexual merozoites are lost by natural death at a rate of μ_m and are removed by their invasion of susceptible RBC.

After all the initially injected iRBC have matured or died ($t > \alpha$), the next cohort of asexual iRBC starts to reach maturity. Transmission investment is defined as the proportion, c, of this new generation that commits to gametocytogenesis, resulting in the production of β sexually-committed merozoites (M_g) per cell. These sexual merozoites invade susceptible RBCs to produce sexual iRBCs (I_g). We assume that sexually-committed merozoites have the same death rate (μ_m) and rate of RBC invasion (ϵ) as asexual merozoites. The remaining proportion ($1 - c$) of iRBC produces asexual merozoites and continues the asexual replication cycle. Altogether, when $t > \alpha$, the dynamics of iRBC and merozoites are as follows:

$$\frac{dI}{dt} = \underbrace{\epsilon R(t)M(t)}_{\text{RBC invasion}} - \underbrace{\mu I(t)}_{\text{Natural death}} - \underbrace{[-ln(1-N(t)) - ln(1-W(t))]I(t)}_{\text{Indiscriminate and targeted immunity}} - \underbrace{\epsilon R(t-\alpha)M(t-\alpha)S}_{\text{iRBC maturation}} \tag{4}$$

$$\frac{dM}{dt} = \underbrace{\beta(1-c)\epsilon R(t-\alpha)M(t-\alpha)S}_{\text{iRBC maturation (asexual)}} - \underbrace{\mu_m M(t)}_{\text{Natural death}} - \underbrace{\epsilon R(t)M(t)}_{\text{RBC invasion}} \tag{5}$$

$$\frac{dM_g}{dt} = \underbrace{\beta c\epsilon R(t-\alpha)M(t-\alpha)S}_{\text{iRBC maturation (sexual)}} - \underbrace{\mu_m M_g(t)}_{\text{Natural death}} - \underbrace{\epsilon R(t)M_g(t)}_{\text{RBC invasion}}. \tag{6}$$

The parameter governing transmission investment (c), which represents the proportion of iRBCs that produce sexually-committed merozoites, is determined by a transformed cue variable, f_t, perceived by the parasite infecting a cell perceived α days ago to account for NCC ($f_t(t-\alpha)$). Following the approach taken by Greischar *et al.* [20], we modeled the transmission investment reaction norm as the complementary log-log basis-spline with three degrees of freedom (B_3). The complementary log-log is applied to constrain investment between zero and one. For numerical optimization, the perceived cue must be within the bound of the reaction norm. To achieve this, the perceived cue variable $f(t-\alpha)$ governing transmission investment is transformed via a linear combination of Heaviside step functions (H) from the R package *CRONE* [86] that set all negative values to zero and limit values to a predefined maximum (max). In summary, the transmission investment function is defined as

$$c[f_t(t-\alpha)] = exp(-exp(B_3[f_t(t-\alpha)])), \tag{7}$$

where the Heaviside-transformed environmental cue $f_t(t-\alpha)$ is given by

$$f_t(t-\alpha) = H[f(t-\alpha)]f(t-\alpha) + H[f(t-\alpha) - \max][\max - f(t-\alpha)]. \tag{8}$$

For the model that incorporates dual cue perception, we used the *mgcv* package [87] to model transmission investment as the response variable of a generalized additive model. This model incorporates a full tensor product smooth of two environmental cues with nine degrees of freedom, represented as follows:

$$c[f_{t1}(t-\alpha), f_{t2}(t-\alpha)] = exp(-exp(\sum_{i=1}^{3}\sum_{j=1}^{3}\zeta_{ij}\beta_3[f_{t1}(t-\alpha)]\beta_3[f_{t2}(t-\alpha)])), \tag{9}$$

where transmission investment is governed by two Heaviside-transformed cues, f_{t1} and f_{t2}, perceived α days ago. The transmission investment surface (i.e., 2-dimensional reaction norm) is generated by taking the tensor product of the basis-splines (β_3) of two cues. The shape of this spline surface is defined by the model coefficients ζ_{ij}.

Before the first cohort of sexual iRBC matures ($\alpha < t \leq \alpha + \alpha_g$), the dynamics of sexual iRBC is governed solely by the rate of RBC invasion by sexually-committed merozoites, natural RBC death, and immunity:

$$\frac{dI_g}{dt} = \underbrace{\epsilon R(t) M_g(t)}_{\text{RBC invasion}} - \underbrace{\mu I_g(t)}_{\text{Natural death}} - \underbrace{[-ln(1-N(t)) - ln(1-W(t))] I_g(t)}_{\text{Indiscriminate and targeted immunity}}. \tag{10}$$

When the first cohort of sexual iRBC matures ($t > \alpha + \alpha_g$), each sexual iRBC produces a single gametocyte, G, such that

$$\begin{aligned}\frac{dI_g}{dt} = & \underbrace{\epsilon R(t) M_g(t)}_{\text{RBC invasion}} - \underbrace{\mu I_g(t)}_{\text{Natural death}} - \underbrace{[-ln(1-N(t)) - ln(1-W(t))] I_g(t)}_{\text{Indiscriminate and targeted immunity}} \\ & - \underbrace{\epsilon R(t-\alpha_g) M_g(t-\alpha_g) S_g}_{\text{iRBC maturation (sexual)}},\end{aligned} \tag{11}$$

$$\frac{dG}{dt} = \underbrace{\epsilon R(t-\alpha_g) M_g(t-\alpha_g) S_g}_{\text{iRBC maturation (sexual)}} - \underbrace{\mu_g G(t)}_{\text{Natural death}}, \tag{12}$$

where μ_g is the background death rate of gametocytes. The survival probability of sexual iRBCs during their development cycle is defined by the exponential survival function S_g, which is similar to that of asexual iRBC (S), except the cumulative hazard function is integrated over the length of sexual iRBC development, α_g:

$$S_g = exp[-\int_{t-\alpha_g}^{t} \underbrace{\mu}_{\text{Natural death}} \underbrace{-ln(1-N(\omega)) - ln(1-W(\omega))}_{\text{Indiscriminate and targeted immunity}} d\omega]. \tag{13}$$

Throughout the infection, indiscriminate immunity eliminates RBC and iRBC whereas targeted immunity eliminates only iRBC; we define N and W as the proportion of RBCs and iRBCs cleared per day, respectively. The magnitude of this activity is dependent on the total amount of iRBC, as detailed in Kamiya *et al.* [43]:

$$\frac{dN}{dt} = \underbrace{\psi_n \frac{I(t) + I_g(t)}{\iota}(1 - N(t))}_{\text{Immune activation}} - \underbrace{\frac{N(t)}{\phi_n}}_{\text{Immune decay}} \tag{14}$$

$$\frac{dW}{dt} = \underbrace{\psi_w \frac{I(t) + I_g(t)}{\iota}(1 - W(t))}_{\text{Immune activation}} - \underbrace{\frac{W(t)}{\phi_w}}_{\text{Immune decay}}, \tag{15}$$

where ψ_n and ψ_w denote the immune activation strengths, ϕ_n and ϕ_w represent the immune activity half-lives, and ι represents the theoretical maximum total iRBC density, which determines the threshold at which immunity saturates. Experimental data from mouse infections indicate that indiscriminate immunity is quickly activated but short-lived, whereas targeted immunity has a longer activation period but a longer half-life [43].

Throughout the infection, the density of uninfected RBCs, R, is affected by erythropoiesis, natural death, indiscriminate immunity, and merozoite invasion, such that:

$$\frac{dR}{dt} = \underbrace{\mu R_0}_{\text{Erythropoiesis}} + \underbrace{\rho(R_0 - R(t))}_{\text{Erythropoiesis upregulation}} - \underbrace{\mu R(t)}_{\text{Natural death}} - \underbrace{[-ln(1 - N(t))R(t)]}_{\text{Indiscriminate immunity}} - \underbrace{\epsilon R(t)[M(t) + M_g(t)]}_{\text{Merozoite invasion}}. \tag{16}$$

In the absence of parasites, RBCs are replenished at a baseline rate that maintains a homeostatic equilibrium RBC concentration (R_0). During infection, the rate of erythropoiesis increases, and the extent of this upregulation is proportional to the deviation of RBC concentration from equilibrium [88], where ρ represents the maximum proportion of the RBC deficit recovered per day. RBCs are eliminated at a natural death rate of μ, removed through indiscriminate immunity ($-ln(1 - N(t))$), or converted to iRBC via invasion by merozoites.

Quantifying parasite fitness

To quantify parasite fitness, we calculated the cumulative transmission potential of different transmission investment strategies, following the method described by Greischar *et al.* [20]. For a given time step, transmission potential, $\tau(t)$, is defined as the probability that a mosquito vector becomes infected after biting an infected host and has been shown empirically to be a sigmoid function of gametocyte density in this parasite species [9],

$$\tau(t) = \frac{e^{-12.69+3.6\log_{10}(G(t))}}{1 + e^{-12.69+3.6\log_{10}(G(t))}}. \tag{17}$$

The cumulative transmission potential, or overall fitness of the parasite, is calculated by integrating transmission potential over the entire infection duration of δ days:

$$\text{fitness} = \int_0^{\delta} \tau(\omega) d\omega. \tag{18}$$

This fitness metric assumes that the mosquito population is at a constant abundance and continuously biting, for the duration of the infection. Although this is a simplification of the evolutionary pressures faced by malaria parasites [22], it enables us to focus our investigation at the within-host level, where transmission investment "decisions" are being made and environmental cues are being perceived by parasites. In our numerical simulations, we estimated fitness with a step size of 0.001 days unless stated otherwise.

Cue choice and perception

Transmission investment has been shown to vary in response to within-host competition [10] and reticulocyte proportion (young RBC) for *P. chabaudi* [29], lysophosphatidylcholine level (a key component of the RBC plasma membrane) and exosome-like particles for *P. falciparum* [89, 90]. Whether parasites are responding to these cues directly, or if they are instead a proxy for changes in some other within-host environmental factor is unclear. To capture some of the diversity of putative cues, we defined transmission investment as a function of ten different host and parasite-centric cues (Table 3). Additionally, we implemented dual cue models, allowing parasites to simultaneously perceive two different cues. As transmission investment in *P. falciparum*

varies non-linearly with lysophosphatidylcholine concentration [89], and within-host dynamics are known to vary only when infectious dose changes by orders of magnitude [24], we introduced non-linear cue perception, enabling parasites to perceive cues either unaltered or $\log_{10}$-transformed. We excluded merozoite density as a cue due to its short half-life and the rapid pace of RBC invasion [91]. We also did not include measurements of immunity as cues, given that our model does not track individual components of immunity (rather, it tracks immune killing, phenomenologically), nor do we have sufficient empirical evidence detailing the relationship between different immunity components and transmission investment.

Table 3. Within-host environmental cues tested and their range.

Cue (density per μL)	Abbreviation	Min. value	Max. value
Asexual iRBC	I	0	$6x10^6$
Asexual iRBC $\log_{10}$	I log	0	6.78
Sexual iRBC	Ig	0	$6x10^6$
Sexual iRBC $\log_{10}$	Ig log	0	6.78
Asexual iRBC + sexual iRBC	Total I	0	$6x10^6$
Asexual iRBC $\log_{10}$ + sexual iRBC $\log_{10}$	Total I log	0	6.78
Gametocyte	G	0	$6x10^4$
Gametocyte $\log_{10}$	G log	0	4.78
RBC	R	10^6	10^7
RBC $\log_{10}$	R log	6	7

For all cues, we adopt a standardized range that spans the values typically observed when infecting immunologically naive mice with *P. chabaudi* [12], given by the minimum and maximum values in Table 3. All values that exceed the maximum bounds are "perceived" by the parasite as the maximum bound via the modified Heaviside transformation function.

Fitness optimization

Acute *P. chabaudi* infection tends to resolve within 20 days [92]. For all models, we therefore confined our simulations and optimizations to a 20-day infection period using the parameters detailed in Table 2 and using the *deSolve* package in R [93]. To ensure the convergence and continuity of output dynamics, we simulated the models with a small time step size of 0.001 days using the vode solver [94]. For the dual cue model, we used a larger time step of 0.01 days (which does not greatly alter parasite dynamics but improves computational speed immensely).

To investigate how transmission investment strategies affect parasite fitness, we performed numerical optimization of the basis-spline (single cue) or generalized additive model coefficients (dual cue) to maximize the cumulative transmission potential. We optimized the models using two methods to increase the chances of obtaining the global fitness optima. First, we performed local optimization following the methodology outlined by Greischar *et al.* [20] with the same arbitrary initial values of all 0.5 for all spline coefficients, but using the more efficient parallelized L-BFGS-B algorithm (Limited-Memory Broyden–Fletcher–Goldfarb–Shanno algorithm-B) implemented in the *OptimParallel* package [95]. Second, we optimized each model using a hybrid approach to avoid convergence to a local fitness maximum. This technique involved initial global optimization using the Differential Evolution (DE) algorithm from the *DEoptim* package [96] (maximum iterations = 500, step tolerance = 50, differential weighting

factor = 0.8, cross-over constant = 0.5 (single cue) or 0.9 (dual cue), population size = 40 (single cue) or 90 (dual cue), time step = 0.01 (single cue) or 0.05 (dual cue)). DE is an efficient and robust algorithm with comparable/better performance relative to other stochastic optimization algorithms [97]. Following optimization by the Differential Evolution algorithm, we further optimized the objective function using the L-BFGS-B algorithm to pinpoint a probable fitness maximum. For the single cue models, the local optimization is performed with a time step of 0.001 days while the dual cue model uses a time step of 0.01 days due to computational constraints. For the differential Evolution algorithm, we used a parameter bound of $(-5, -500, -500, -500)$ and $(5, 500, 5000, 500)$ for the single cue model and (-10, -500, -1000, -1000, -250, -500, -1000, -500, -250) and (10, 500, 1000, 1000, 250, 500, 1000, 500, 250) for the dual cue model. These bounds effectively encompass the majority of basis-spline flexibility. From the two optimization results, we selected the parameter sets that resulted in the highest fitness.

As a further validation step, we compared the fitness of each putative single cue optimal strategy to the fitness obtained by 1000 randomly generated strategies. These random strategies were generated within the predefined bounds of $(-5, -500, -500, -500)$ and $(5, 500, 5000, 500)$, established previously to encompass much of the spline space.

Semi-stochastic infection model

In order to explore the impact of individual infection-level variation on putative optimal transmission investment strategies, we incorporated the following random variables in the within-host model: maximum proportion of RBC deficit recovered per day (ρ), parasite burst size (β), immunity activation strengths (ψ_n and ψ_w), and immunity half-lives (ϕ_n and ϕ_w). For each iteration, random variables were drawn from 167 Markov chains (selected at regular intervals from a pool of 16,000 chains) used to estimate the posterior distribution. For the maximum proportion of RBC recovered per day and parasite burst size, the posterior distributions (originally centered at zero; from [43]) are re-centered at the deterministic model values of 0.263 and 5.721, respectively. Since the paper from which we draw parameters explored the impact of dose [43], we only considered estimates pertaining to hosts infected with an initial dose of 10^4 parasites (constituting around 1000 parameter values), which corresponds to our choice for this model parameter (Table 2).

For each optimal transmission investment strategy (i.e., the best strategy for each cue or cues combination), we performed 20-day simulations with (i) all parameters allowed to vary from their deterministic default and (ii) only a single parameter varying. Here, we used a time step of 0.01 days, which does not change fitness substantially relative to performing the simulation with a time step of 0.001 days. The contribution of variation in individual parameters to the total variation in fitness observed when all parameters varied is quantified as:

$$\text{relative fitness perturbation[i]} = \frac{\text{fitness}_{single}[i] - \text{fitness}_{det}}{\text{fitness}_{all}[i] - \text{fitness}_{det}}, \tag{19}$$

where fitness_{single} represents the fitness value derived at the ith trial with only one parameter varying, fitness_{det} represents the fitness value derived from the deterministic model, and fitness_{all} represents the fitness value derived when all six parameters are varying.

Disease mapping of laboratory mice infections

To explore the dynamics of host and parasite-centric cues in an *in vivo* setting, we curated data from publicly available sources of *P. chabaudi* infection dynamics in mice [12, 30–33]. The curated dataset includes experiments that met the following criteria: a) single parasite strain infection, b) no administration of anti-malarial drugs, and c) availability of data on iRBC, RBC, and gametocyte densities. We then visualized two-dimensional disease maps (iRBC vs. RBC path plots) using the R package *ggplot2* [98].

Quantifying parasite virulence

We used the area encompassed within a disease map (where the x-axis displays total iRBC density and the y-axis displays uninfected RBC density) as a proxy for parasite virulence. To calculate this area, we first used the *chull* function [99] to define the convex hull (a set of coordinates that define the smallest area that captures all of the points within the infection trajectory). We then used the *areapl* function from the *splancs* package [100] to quantify the area of the convex hull.

Supporting information

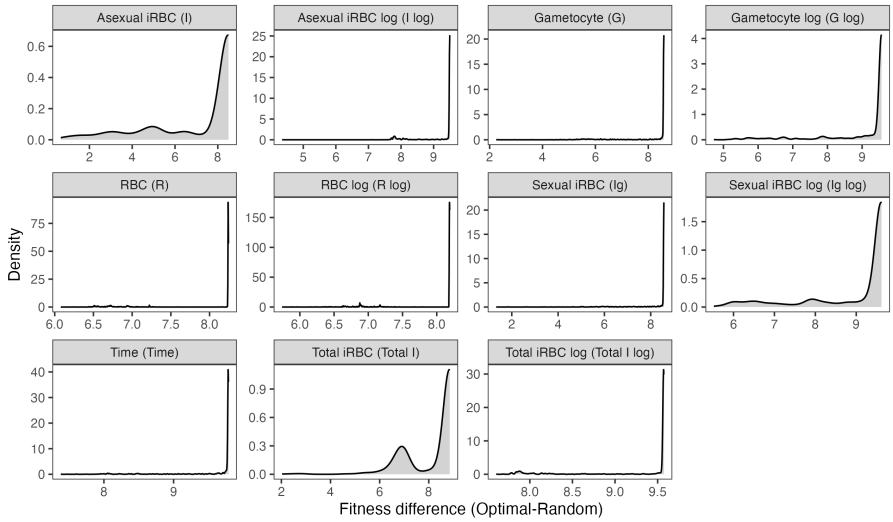

S1 Fig. Validation of transmission investment optimization. We conducted 1000 infection simulations for parasites sensing different cues, with each simulation using randomly generated transmission investment strategies. The fitness values of these simulations were compared to the fitness of parasites adopting the optimal transmission investment strategy. Each histogram represents the difference between the optimized fitness and the fitness obtained from the randomly generated strategy. The fitness of the random strategies is always lower.

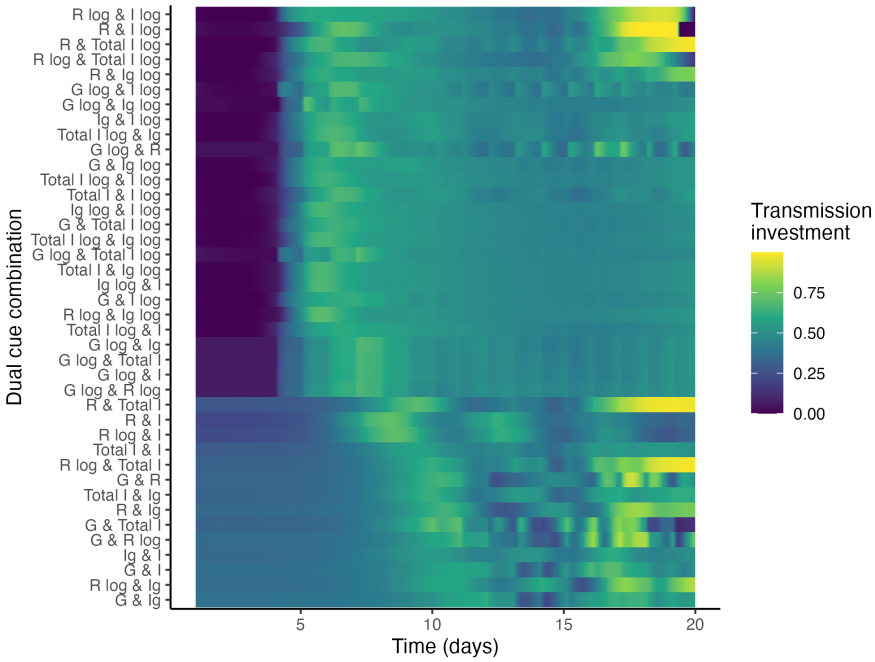

S2 Fig. Transmission investment dynamics produced by parasites sensing different dual cue combinations. Transmission investment is plotted for all possible dual cue combinations, with heatmaps ranked in descending order (from top to bottom) based on their associated cumulative transmission potential.

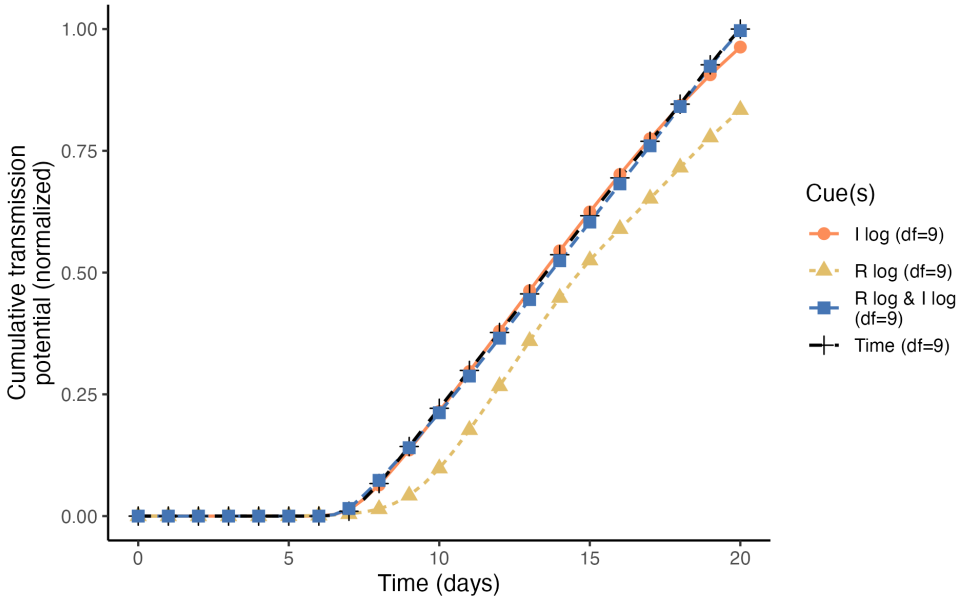

S3 Fig. Terminal investment increases the fitness of dual cue-perceiving parasites. The cumulative transmission potential of parasites sensing time, the best performing dual cue combination (R log & I log), or the individual single cues (I log, R log) are indicated with a black cross, blue square, orange circle, and yellow triangle, respectively. The cumulative transmission potential is normalized to the fitness of the

with respect to the best time-varying strategy. Note that time, the dual cue combination, and I log all permit an initial delay in transmission investment, while R log does not; the fitness advantage of this delayed strategy can be clearly viewed on these plots. Only time and the dual cue combination lead to terminal investment, leading to additional fitness gains from day 18 onward.

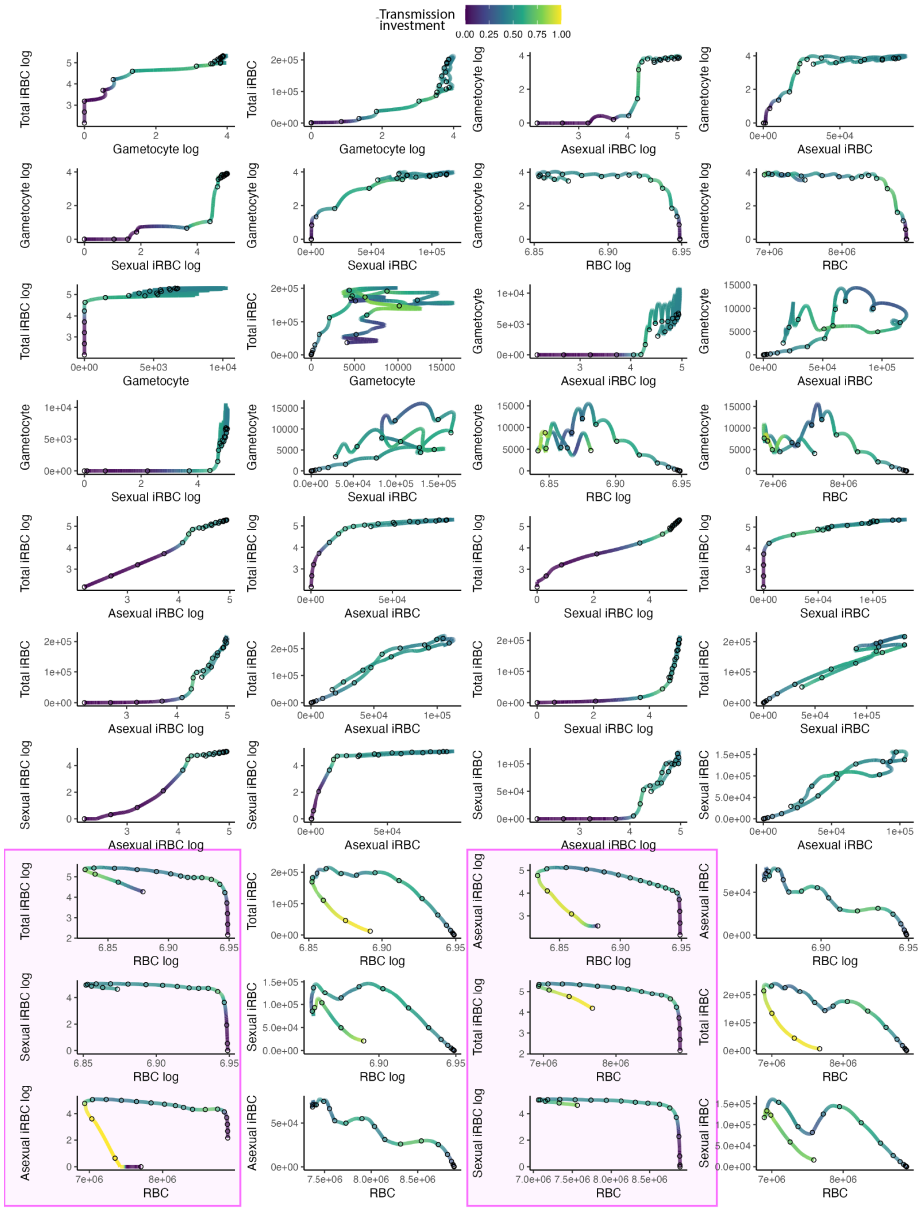

S4 Fig. RBC/logged RBC and logged iRBC form a looping trajectory *in silico*. Graphs display the two-dimensional reaction norm and infection trajectories for parasites sensing all dual cue combinations. The trajectories depict the dynamics of the cues (indicated on the x- and y-axes) along with the corresponding transmission investment (represented by the color of the line) when parasites adopt the optimal strategy for each cue combination. The distance between each hollow circle represents one day. Cue combinations that form a prominent loop, where each day maps to a

unique coordinate, are highlighted with a pink box.

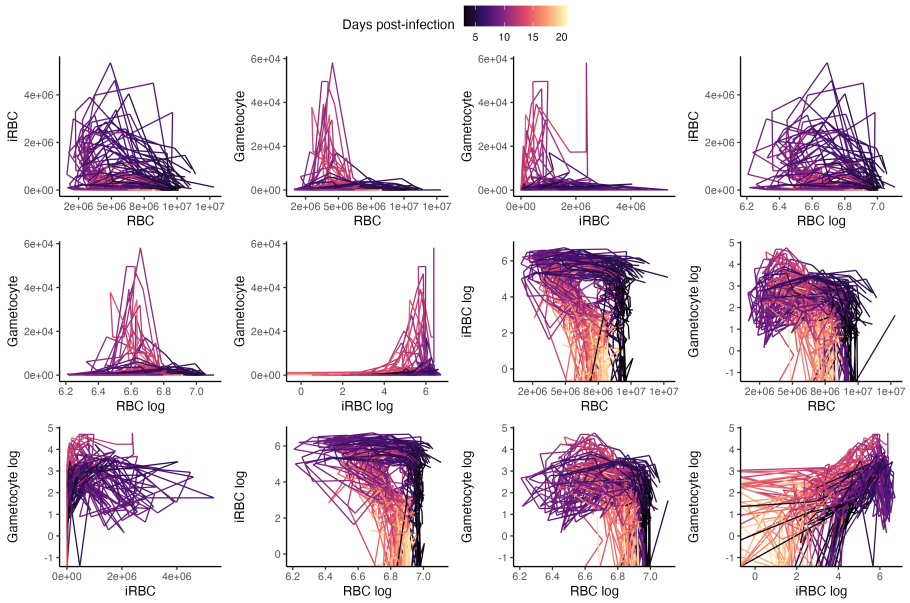

S5 Fig. RBC/logged RBC and logged iRBC form a looping trajectory *in vivo*. To identify combinations of within-host variables that exhibit a looping relationship, we plotted all possible permutations of experimentally derived *P. chabaudi* variables. Each line represents the dynamics of a single strain of infecting parasite. The line colour indicates the progression of time.

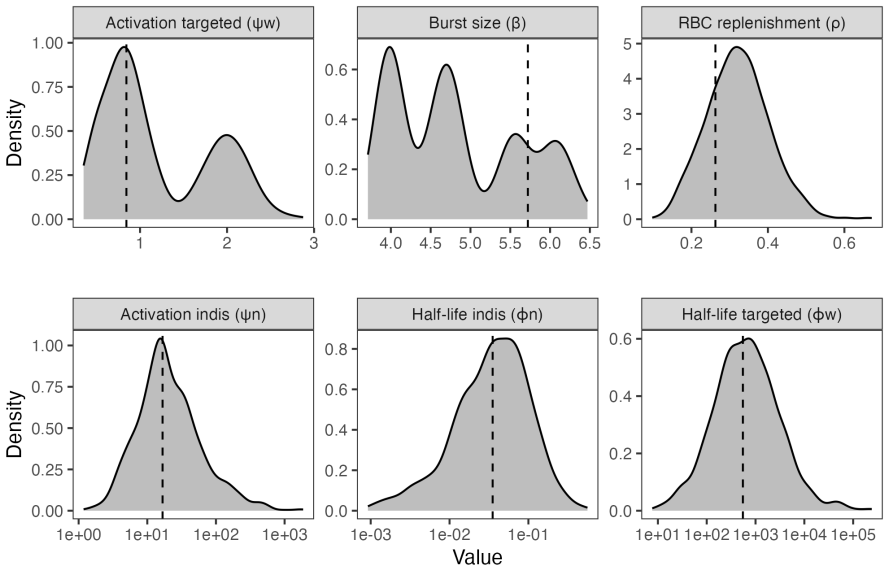

S6 Fig. Posterior distribution of parameter values used for the semi-stochastic model. The histograms display the distribution of 1000 parameter values drawn from 167 Markov chains derived by Kamiya *et al* [43]. The parameter values used in the deterministic model are indicated by the dotted line.

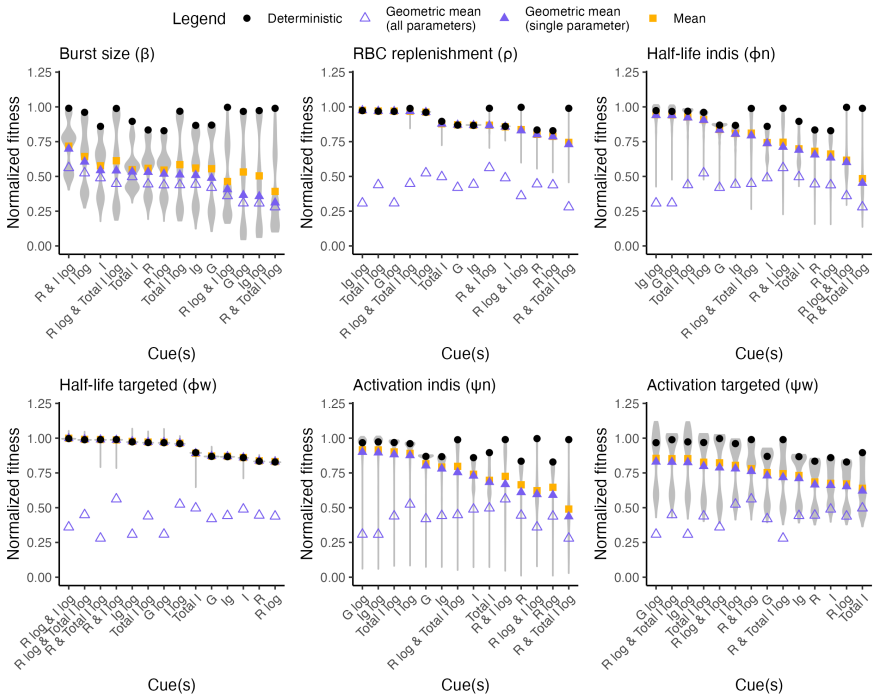

S7 Fig. Distribution of parasite fitness when one parameter is varying. We conducted 1000 simulations, each lasting 20 days, in which parasites adopted the optimal transmission investment strategy (from the deterministic model) using a semi-stochastic model where only one parameter was randomly drawn from the posterior distributions (see S6 Fig). The distribution of fitness values is displayed as a grey violin plot. Summary statistics are represented as follows: fitness from the deterministic model (black circle), geometric mean fitness when all six parameters are varied (hollow purple triangle), geometric mean fitness when one parameter is varied (solid purple triangle), and mean fitness when one parameter is varied (yellow square). The varied parameter is indicated at the top of each graph, with cues ranked by descending geometric mean fitness when one parameter is varied. When burst size is varied, the deterministic fitness (black circle) is largely uncoupled from the fitness in the semi-stochastic model (open triangles). When other parameters are varied, the deterministic model fitness is associated with the fitness from the semi-stochastic model except for parasites sensing dual cues, which experiences higher fitness loss with parameter variations.

Acknowledgments

We thank members of the Mideo Lab for their useful feedback on the project.

References

1. Jones OR, Scheuerlein A, Salguero-Gómez R, Camarda CG, Schaible R, Casper BB, et al. Diversity of ageing across the tree of life. Nature. 2014;505(7482):169–173. doi:10.1038/nature12789.

2. Gadgil M, Bossert WH. Life Historical Consequences of Natural Selection. The American Naturalist. 1970;104(935):1–24. doi:10.1086/282637.

3. Clutton-Brock TH, Albon SD, Guinness FE. Maternal dominance, breeding success and birth sex ratios in red deer. 1984;308(5957):358–360. doi:https://doi.org/10.1038/308358a0.

4. McNamara JM, Houston AI. State-dependent life histories. Nature. 1996;380(6571):215–221. doi:10.1038/380215a0.

5. Cotter SC, Ward RJS, Kilner RM. Age-specific reproductive investment in female burying beetles: independent effects of state and risk of death. Functional Ecology. 2011;25(3):652–660. doi:10.1111/j.1365-2435.2010.01819.x.

6. Velando A, Drummond H, Torres R. Senescent birds redouble reproductive effort when ill: confirmation of the terminal investment hypothesis. Proceedings of the Royal Society B: Biological Sciences. 2006;273(1593):1443–1448. doi:10.1098/rspb.2006.3480.

7. Churcher TS, Bousema T, Walker M, Drakeley C, Schneider P, Ouédraogo AL, et al. Predicting mosquito infection from *Plasmodium falciparum* gametocyte density and estimating the reservoir of infection. eLife. 2013;2:e00626. doi:10.7554/eLife.00626.

8. Bell AS, Huijben S, Paaijmans KP, Sim DG, Chan BHK, Nelson WA, et al. Enhanced Transmission of Drug-Resistant Parasites to Mosquitoes following Drug Treatment in Rodent Malaria. PLOS ONE. 2012;7(6):e37172. doi:10.1371/journal.pone.0037172.

9. Huijben S, Nelson WA, Wargo AR, Sim DG, Drew DR, Read AF. Chemotherapy, within-host ecology and the fitness of drug-resistant malaria parasites. Evolution. 2010;64(10):2952–2968. doi:10.1111/J.1558-5646.2010.01068.X.

10. Carter LM, Kafsack BFC, Llinás M, Mideo N, Pollitt LC, Reece SE. Stress and sex in malaria parasites: Why does commitment vary? Evolution, Medicine, and Public Health. 2013;2013(1):135–147. doi:10.1093/EMPH/EOT011.

11. Clutton-Brock TH. Reproductive Effort and Terminal Investment in Iteroparous Animals. https://doiorg/101086/284198. 2015;123(2):212–229. doi:10.1086/284198.

12. Pollitt LC, Mideo N, Drew DR, Schneider P, Colegrave N, Reece SE. Competition and the Evolution of Reproductive Restraint in Malaria Parasites. https://doiorg/101086/658175. 2011;177(3):358–367. doi:10.1086/658175.

13. Eichner M, Diebner HH, Molineaux L, Collins WE, Jeffery GM, Dietz K. Genesis, sequestration and survival of *Plasmodium falciparum* gametocytes: parameter estimates from fitting a model to malariatherapy data. Transactions of The Royal Society of Tropical Medicine and Hygiene. 2001;95(5):497–501. doi:10.1016/S0035-9203(01)90016-1.

14. Cameron A, Reece SE, Drew DR, Haydon DT, Yates AJ. Plasticity in transmission strategies of the malaria parasite, *Plasmodium chabaudi*: environmental and genetic effects. Evolutionary Applications. 2013;6(2):365. doi:10.1111/EVA.12005.

15. Greischar MA, Mideo N, Read AF, Bjørnstad ON. Quantifying Transmission Investment in Malaria Parasites. PLOS Computational Biology. 2016;12(2):e1004718. doi:10.1371/JOURNAL.PCBI.1004718.

16. Reece SE, Ramiro RS, Nussey DH. Synthesis: Plastic parasites: sophisticated strategies for survival and reproduction? Evolutionary Applications. 2009;2(1):11–23. doi:10.1111/j.1752-4571.2008.00060.x.

17. Pianka ER, Parker WS. Age-Specific Reproductive Tactics. The American Naturalist. 1975;109(968):453–464. doi:10.1086/283013.

18. McKenzie FE, Bossert WH. An integrated model of *Plasmodium falciparum* dynamics. Journal of Theoretical Biology. 2005;232(3):411–426. doi:10.1016/j.jtbi.2004.08.021.

19. Bousema T, Drakeley C. Epidemiology and infectivity of *Plasmodium falciparum* and *Plasmodium vivax* gametocytes in relation to malaria control and elimination. Clinical Microbiology Reviews. 2011;24(2):377–410. doi:10.1128/CMR.00051-10.

20. Greischar MA, Mideo N, Read AF, Bjørnstad ON. Predicting optimal transmission investment in malaria parasites. Evolution. 2016;70(7):1542–1558. doi:10.1111/EVO.12969.

21. Cao P, Collins KA, Zaloumis S, Wattanakul T, Tarning J, Simpson JA, et al. Modeling the dynamics of *Plasmodium falciparum* gametocytes in humans during malaria infection. eLife. 2019;8:e49058. doi:10.7554/eLife.49058.

22. Greischar MA, Beck-Johnson LM, Mideo N. Partitioning the influence of ecology across scales on parasite evolution. Evolution. 2019;73(11):2175–2188. doi:10.1111/EVO.13840.

23. Early AM, Camponovo F, Pelleau S, Cerqueira GC, Lazrek Y, Volney B, et al. Declines in prevalence alter the optimal level of sexual investment for the malaria parasite *Plasmodium falciparum*. Proceedings of the National Academy of Sciences. 2022;119(30):e2122165119. doi:10.1073/pnas.2122165119.

24. Timms R, Colegrave N, Chan BHK, Read AF. The effect of parasite dose on disease severity in the rodent malaria *Plasmodium chabaudi*. Parasitology. 2001;123(Pt 1):1–11. doi:10.1017/S0031182001008083.

25. Lensen A, Bril A, van de Vegte M, van Gemert GJ, Eling W, Sauerwein R. *Plasmodium falciparum*: infectivity of cultured, synchronized gametocytes to mosquitoes. Experimental Parasitology. 1999;91(1):101–103. doi:10.1006/expr.1998.4354.

26. Dixon MWA, Thompson J, Gardiner DL, Trenholme KR. Sex in *Plasmodium*: a sign of commitment. Trends in Parasitology. 2008;24(4):168–175. doi:10.1016/J.PT.2008.01.004.

27. Birget PLG, Greischar MA, Reece SE, Mideo N. Altered life history strategies protect malaria parasites against drugs. Evolutionary Applications. 2018;11(4). doi:10.1111/eva.12516.

28. Mantel PY, Hoang A, Goldowitz I, Potashnikova D, Hamza B, Vorobjev I, et al. Malaria-Infected Erythrocyte-Derived Microvesicles Mediate Cellular Communication within the Parasite Population and with the Host Immune System. Cell Host & Microbe. 2013;13(5):521–534. doi:10.1016/J.CHOM.2013.04.009.

29. Birget PLG, Repton C, O'Donnell AJ, Schneider P, Reece SE. Phenotypic plasticity in reproductive effort: malaria parasites respond to resource availability. Proceedings of the Royal Society B: Biological Sciences. 2017;284(1860). doi:10.1098/RSPB.2017.1229.

30. Huijben S, Sim DG, Nelson WA, Read AF. Data from: The fitness of drug-resistant malaria parasites in a rodent model: multiplicity of infection. Dryad. 2011;.

31. Huijben S, Nelson WA, Wargo AR, Sim DG, Drew DR, Read AF. Data from: Chemotherapy, within-host ecology and the fitness of drug-resistant malaria parasites. Dryad. 2013;.

32. Huijben S, Bell AS, Sim DG, Tomasello D, Mideo N, Day T, et al. Data from: Aggressive chemotherapy and the selection of drug resistant pathogens. Dryad. 2014;.

33. Huijben S, Chan BHK, Nelson WA, Read AF. Data from: The impact of within-host ecology on the fitness of a drug-resistant parasite. Dryad. 2018;.

34. Torres BY, Oliveira JHM, Thomas Tate A, Rath P, Cumnock K, Schneider DS. Tracking Resilience to Infections by Mapping Disease Space. PLOS Biology. 2016;14(4):e1002436. doi:10.1371/JOURNAL.PBIO.1002436.

35. Moran NA. The Evolutionary Maintenance of Alternative Phenotypes. The American Naturalist. 1992;139(5):971–989. doi:10.1086/285369.

36. Scheiner SM. The genetics of phenotypic plasticity. VII. Evolution in a spatially-structured environment. Journal of Evolutionary Biology. 1998;11(3):303–320. doi:10.1046/j.1420-9101.1998.11030303.x.

37. De Jong G. Unpredictable selection in a structured population leads to local genetic differentiation in evolved reaction norms. Journal of Evolutionary Biology. 1999;12(5). doi:10.1046/j.1420-9101.1999.00118.x.

38. Schlaepfer MA, Runge MC, Sherman PW. Ecological and evolutionary traps. Trends in Ecology & Evolution. 2002;17(10):474–480. doi:10.1016/S0169-5347(02)02580-6.

39. Reed TE, Robin SW, Schindler DE, Hard JJ, Kinnison MT. Phenotypic plasticity and population viability: The importance of environmental predictability. Proceedings of the Royal Society B: Biological Sciences. 2010;277(1699). doi:10.1098/rspb.2010.0771.

40. Tufto J. The evolution of plasticity and nonplastic spatial and temporal adaptations in the presence of imperfect environmental cues. American Naturalist. 2000;156(2). doi:10.1086/303381.

41. Antia R, Yates A, de Roode JC. The dynamics of acute malaria infections. I. Effect of the parasite's red blood cell preference. Proceedings of the Royal Society B: Biological Sciences. 2008;275(1641):1449–1458. doi:10.1098/rspb.2008.0198.

42. Birget PLG, Kimberley F Prior, Savill NJ, Steer L, Reece SE. Plasticity and genetic variation in traits underpinning asexual replication of the rodent malaria parasite, *Plasmodium chabaudi*. Malaria Journal. 2019;18(1):222. doi:10.1186/s12936-019-2857-0.

43. Kamiya T, Greischar MA, Schneider DS, Mideo N. Uncovering drivers of dose-dependence and individual variation in malaria infection outcomes. PLOS Computational Biology. 2020;16(10):e1008211. doi:10.1371/JOURNAL.PCBI.1008211.

44. Haydon DT, Matthews L, Timms R, Colegrave N. Top-down or bottom-up regulation of intra-host blood-stage malaria: do malaria parasites most resemble the dynamics of prey or predator? Proceedings of the Royal Society B: Biological Sciences. 2003;270(1512):289–298. doi:10.1098/rspb.2002.2203.

45. Miller MR, Råberg L, Read AF, Savill NJ. Quantitative Analysis of Immune Response and Erythropoiesis during Rodent Malarial Infection. PLOS Computational Biology. 2010;6(9):e1000946. doi:10.1371/JOURNAL.PCBI.1000946.

46. Kamiya T, Davis NM, Greischar MA, Schneider D, Mideo N. Linking functional and molecular mechanisms of host resilience to malaria infection. eLife. 2021;10. doi:10.7554/ELIFE.65846.

47. Nijhout HF. A Developmental-Physiological Perspective on the Development and Evolution of Phenotypic Plasticity. In: Love AC, editor. Conceptual Change in Biology: Scientific and Philosophical Perspectives on Evolution and Development. Boston Studies in the Philosophy and History of Science. Dordrecht: Springer Netherlands; 2014. p. 147–173. Available from: `https://doi.org/10.1007/978-94-017-9412-1_7`.

48. Lewontin RC, Cohen D. On population growth in a randomly varying environment. Proceedings of the National Academy of Sciences of the United States of America. 1969;62(4):1056–1060. doi:10.1073/pnas.62.4.1056.

49. Gillespie J. Polymorphism in random environments. Theoretical Population Biology. 1973;4(2):193–195. doi:10.1016/0040-5809(73)90028-2.

50. Pak D, Kamiya T, Greischar MA. Proliferation in malaria parasites: How resource limitation can prevent evolution of greater virulence. Evolution. 2024;78(7):1287–1301. doi:10.1093/evolut/qpae057.

51. Schneider P, Reece SE. The private life of malaria parasites: Strategies for sexual reproduction. Molecular and Biochemical Parasitology. 2021;244:111375. doi:10.1016/J.MOLBIOPARA.2021.111375.

52. Schneider P, Greischar MA, Birget PLG, Repton C, Mideo N, Reece SE. Adaptive plasticity in the gametocyte conversion rate of malaria parasites. PLOS Pathogens. 2018;14(11):e1007371. doi:10.1371/JOURNAL.PPAT.1007371.

53. Pigliucci M. Evolution of phenotypic plasticity: where are we going now? Trends in Ecology & Evolution. 2005;20(9):481–486. doi:10.1016/j.tree.2005.06.001.

54. Kochin BF, Bull JJ, Antia R. Parasite Evolution and Life History Theory. PLOS Biology. 2010;8(10):e1000524. doi:10.1371/journal.pbio.1000524.

55. Koella JC, Antia R. Optimal Pattern of Replication and Transmission for Parasites with Two Stages in Their Life Cycle. Theoretical Population Biology. 1995;47(3):277–291. doi:10.1006/tpbi.1995.1012.

56. McKenzie FE, Bossert WH. The Optimal Production of Gametocytes by *Plasmodium falciparum*. Journal of Theoretical Biology. 1998;193(3):419–428. doi:10.1006/jtbi.1998.0710.

57. Mideo N, Day T. On the evolution of reproductive restraint in malaria. Proceedings of the Royal Society B: Biological Sciences. 2008;275(1639):1217–1224. doi:10.1098/RSPB.2007.1545.

58. Charvin G, Oikonomou C, Siggia ED, Cross FR. Origin of Irreversibility of Cell Cycle Start in Budding Yeast. PLOS Biology. 2010;8(1):e1000284. doi:10.1371/journal.pbio.1000284.

59. Melen GJ, Levy S, Barkai N, Shilo B. Threshold responses to morphogen gradients by zero-order ultrasensitivity. Molecular Systems Biology. 2005;1(1):2005.0028. doi:10.1038/msb4100036.

60. Schneider DS. Tracing Personalized Health Curves during Infections. PLOS Biology. 2011;9(9):e1001158. doi:10.1371/journal.pbio.1001158.

61. Buckling A, Crooks L, Read A. *Plasmodium chabaudi:* Effect of Antimalarial Drugs on Gametocytogenesis. Experimental Parasitology. 1999;93(1):45–54. doi:10.1006/expr.1999.4429.

62. Bruce MC, Alano P, Duthie S, Carter R. Commitment of the malaria parasite *Plasmodium falciparum* to sexual and asexual development. Parasitology. 1990;100 Pt 2(2):191–200. doi:10.1017/S0031182000061199.

63. Portugaliza HP, Miyazaki S, Geurten FJ, Pell C, Rosanas-Urgell A, Janse CJ, et al. Artemisinin exposure at the ring or trophozoite stage impacts *Plasmodium falciparum* sexual conversion differently. eLife. 2020;9:1–22. doi:10.7554/ELIFE.60058.

64. Anderson RM, May RM. Coevolution of hosts and parasites. Parasitology. 1982;85(2):411–426. doi:10.1017/S0031182000055360.

65. Alizon S, Hurford A, Mideo N, Van Baalen M. Virulence evolution and the trade-off hypothesis: history, current state of affairs and the future. Journal of Evolutionary Biology. 2009;22(2):245–259. doi:10.1111/j.1420-9101.2008.01658.x.

66. Mackinnon MJ, Read AF. Genetic Relationships between Parasite Virulence and Transmission in the Rodent Malaria *Plasmodium chabaudi*. Evolution. 1999;53(3):689–703. doi:10.1111/j.1558-5646.1999.tb05364.x.

67. Mackinnon MJ, Gaffney DJ, Read AF. Virulence in rodent malaria: host genotype by parasite genotype interactions. Infection, Genetics and Evolution. 2002;1(4):287–296. doi:10.1016/S1567-1348(02)00039-4.

68. Mackinnon MJ, Read AF. The effects of host immunity on virulence–transmissibility relationships in the rodent malaria parasite *Plasmodium chabaudi*. Parasitology. 2003;126(2):103–112. doi:10.1017/S003118200200272X.

69. Paul R, Lafond T, Müller-Graf C, Nithiuthai S, Brey P, Koella J. Experimental evaluation of the relationship between lethal or non-lethal virulence and transmission success in malaria parasite infections. BMC Evolutionary Biology. 2004;4(1):30. doi:10.1186/1471-2148-4-30.

70. Regoes RR, Nowak MA, Bonhoeffer S. Evolution of Virulence in a Heterogeneous Host Population. Evolution. 2000;54(1):64–71. doi:10.1111/j.0014-3820.2000.tb00008.x.

71. Williams PD. New Insights into Virulence Evolution in Multigroup Hosts. The American Naturalist. 2012;179(2):228–239. doi:10.1086/663690.

72. White PS, Choi A, Pandey R, Menezes A, Penley M, Gibson AK, et al. Host heterogeneity mitigates virulence evolution. Biology Letters. 2020;16(1):20190744. doi:10.1098/rsbl.2019.0744.

73. Hawking F, Wilson ME, Gammage K. Evidence for cyclic development and short-lived maturity in the gametocytes of *Plasmodium falciparum*. Transactions of The Royal Society of Tropical Medicine and Hygiene. 1971;65(5):549–559. doi:10.1016/0035-9203(71)90036-8.

74. Padilla DK, Adolph SC. Plastic inducible morphologies are not always adaptive: The importance of time delays in a stochastic environment. Evolutionary Ecology. 1996;10(1):105–117. doi:10.1007/BF01239351.

75. Hoi AG, Greischar MA, Mideo N. Limited impact of within-vector ecology on the evolution of malaria parasite transmission investment. Frontiers in Malaria. 2024;2. doi:10.3389/fmala.2024.1392060.

76. Lazova MD, Ahmed T, Bellomo D, Stocker R, Shimizu TS. Response rescaling in bacterial chemotaxis. Proceedings of the National Academy of Sciences. 2011;108(33):13870–13875. doi:10.1073/pnas.1108608108.

77. Lillie SH, Pringle JR. Reserve carbohydrate metabolism in *Saccharomyces cerevisiae*: responses to nutrient limitation. Journal of Bacteriology. 1980;143(3):1384–1394. doi:10.1128/jb.143.3.1384-1394.1980.

78. Mukherjee S, Bassler BL. Bacterial quorum sensing in complex and dynamically changing environments. Nature reviews Microbiology. 2019;17(6):371–382. doi:10.1038/s41579-019-0186-5.

79. Getty T. The maintenance of phenotypic plasticity as a signal detection problem. The American Naturalist. 1996;148(2):378–385.

80. Ashander J, Chevin LM, Baskett ML. Predicting evolutionary rescue via evolving plasticity in stochastic environments. Proceedings of the Royal Society B: Biological Sciences. 2016;283(1839):20161690. doi:10.1098/rspb.2016.1690.

81. Mideo N, Barclay VC, Chan BHK, Savill NJ, Read AF, Day T. Understanding and predicting strain-specific patterns of pathogenesis in the rodent malaria *Plasmodium chabaudi*. American Naturalist. 2008;172(5):214–238. doi:doi/10.1086/591684.

82. Landau I, Boulard Y. Life Cycles and Morphology. In: Killick-Kendrick R, Peters W, editors. Rodent Malaria. Academic Press; 1978. p. 53–84.

83. Gautret P, Miltgen F, Gantier JC, Chabaud AG, Landau I. Enhanced gametocyte formation by *Plasmodium chabaudi* in immature erythrocytes: Pattern of production, sequestration, and infectivity to mosquitoes. Journal of Parasitology. 1996;82(6). doi:10.2307/3284196.

84. Mideo N, Savill NJ, Chadwick W, Schneider P, Read AF, Day T, et al. Causes of variation in malaria infection dynamics: Insights from theory and data. American Naturalist. 2011;178(6). doi:10.1086/662670.

85. Greischar MA, Read AF, Bjørnstad ON. Synchrony in malaria infections: How intensifying within-host competition can be adaptive. American Naturalist. 2014;183(2). doi:10.1086/674357.

86. Smith E, Evans G, Foadi J. An effective introduction to structural crystallography using 1D Gaussian atoms. European Journal of Physics. 2017;38(6):065501. doi:10.1088/1361-6404/AA8188.

87. Wood SN. mgcv: GAMs and generalized ridge regression for R. R News. 2001;1.

88. Chang KH, Tam M, Stevenson MM. Modulation of the Course and Outcome of Blood-Stage Malaria by Erythropoietin-Induced Reticulocytosis. The Journal of Infectious Diseases. 2004;189(4):735–743. doi:10.1086/381458.

89. Brancucci NMB, Gerdt JP, Wang C, Niz MD, Philip N, Adapa SR, et al. Lysophosphatidylcholine Regulates Sexual Stage Differentiation in the Human Malaria Parasite *Plasmodium falciparum*. Cell. 2017;171(7):1532–1544.e15. doi:10.1016/J.CELL.2017.10.020.

90. Regev-Rudzki N, Wilson DW, Carvalho TG, Sisquella X, Coleman BM, Rug M, et al. Cell-Cell Communication between Malaria-Infected Red Blood Cells via Exosome-like Vesicles. Cell. 2013;153(5):1120–1133. doi:10.1016/J.CELL.2013.04.029.

91. Boyle MJ, Wilson DW, Richards JS, Riglar DT, Tetteh KKA, Conway DJ, et al. Isolation of viable *Plasmodium falciparum* merozoites to define erythrocyte invasion events and advance vaccine and drug development. Proceedings of the National Academy of Sciences of the United States of America. 2010;107(32). doi:10.1073/pnas.1009198107.

92. Stephens R, Culleton RL, Lamb TJ. The contribution of *Plasmodium chabaudi* to our understanding of malaria. Trends in Parasitology. 2012;28(2). doi:10.1016/j.pt.2011.10.006.

93. Soetaert K, Petzoldt T, Setzer RW. Solving Differential Equations in R: Package deSolve. Journal of Statistical Software. 2020;33(9):1–25. doi:10.18637/jss.v033.i09.

94. Brown PN, Byrne GD, Hindmarsh AC. VODE: A Variable-Coefficient ODE Solver. http://dxdoiorg/101137/0910062. 2006;10(5):1038–1051. doi:10.1137/0910062.

95. Gerber F, Furrer R. optimParallel: An R Package Providing a Parallel Version of the L-BFGS-B Optimization Method. The R Journal. 2019;11(1):352–358. doi:10.32614/RJ-2019-030.

96. Mullen KM, Ardia D, Gil DL, Windover D, Cline J. DEoptim: An R package for global optimization by differential evolution. Journal of Statistical Software. 2011;40(6). doi:10.18637/jss.v040.i06.

97. Lampinen J, Storn R. Differential Evolution. In: Onwubolu GC, Babu BV, editors. New Optimization Techniques in Engineering. Studies in Fuzziness and Soft Computing. Berlin, Heidelberg: Springer; 2004. p. 123–166. Available from: `https://doi.org/10.1007/978-3-540-39930-8_6`.

98. Wickham H. ggplot2: Elegant Graphics for Data Analysis. Springer-Verlag New York; 2016. Available from: `https://ggplot2.tidyverse.org`.

99. R Core Team. R: A language and environment for statistical computing; 2021. Available from: https://www.r-project.org/.

100. Bivand R, Rowlingson B, Diggle P, Petris G, Eglen S. splancs: Spatial and Space-Time Point Pattern Analysis; 2024. Available from: https://CRAN.R-project.org/package=splancs.